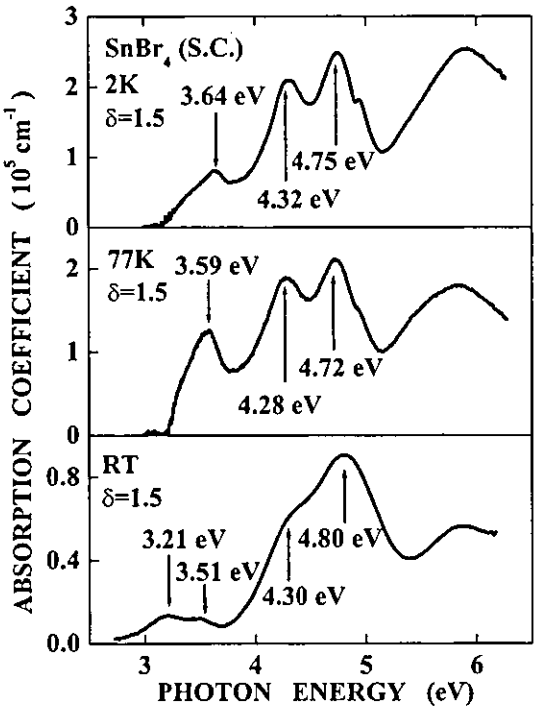

Fig. 1. Absorption spectra of $SnBr_4$ single crystal at 2 K, 77 K and RT. These spectra were derived from the reflection spectra by using Kramers–Kronig formula.

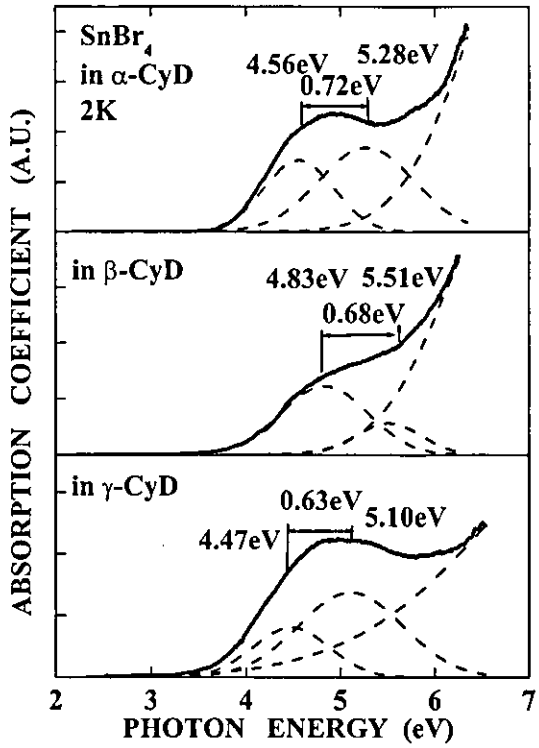

Fig. 2. Absorption spectra of $SnBr_4$ cluster in α-, β- and γ-cyclodextrins at 2 K. These spectra were derived from the reflection spectra of powder sample by using Kubelka–Munk formula.

RT. The exciton absorption band has a small hump at the low energy side at 2 K and 77 K. Another peak was observed at 3.51 eV at RT. The energy difference between 3.21 eV and 3.51 eV is smaller than the spin–orbit coupling constant of bromine (about 0.5 eV). There are two sublattices in a cubic unit cell, therefore, the Davydov splitting would occur. However, the observed splitting energy, 0.30 eV, is bigger than the Davydov splitting. If the peak energies of 3.21 eV and 3.51 eV correspond to 1s and 2s excitons, respectively, the binding energy of 1s exciton is estimated as 0.40 eV by postulating Wannier exciton. The energy gap is estimated as 3.61 eV at RT.

The absorption bands of the spin–orbit split pairs of these exciton bands were not observed. The reasons are as follows: The exciton–phonon coupling is strong in a $SnBr_4$ single crystal and the absorption bands become wide width bands. The split pairs overlap with the higher energy absorption bands and were not clearly distinguished.

There are other higher energy peaks at 4.32 eV and 4.75 eV (2 K), 4.28 eV and 4.78 eV (77 K) and 4.30 eV and 4.80 eV (RT). The energy differences of each pairs are 0.43 eV, 0.44 eV and 0.50 eV, at 2 K, 77 K and RT, respectively. They are close to the spin–orbit coupling energy of bromine. Thus, these absorption pairs come from the transition from the doublet of bromine valence band to the second higher energy conduction band made of tins.

The absorption spectrum of the $SnBr_4$ cluster in a CyD is transformed from the reflectivity spectrum using a Kubelka–Munk formula,

$$A(\lambda) = (1 - R(\lambda))^2/2R(\lambda), \qquad (1)$$

where $A(\lambda)$ is the absorbance and $R(\lambda)$ is the measured diffuse reflectivity at each wavelength.[9] The absorption spectra of the $SnBr_4$ clusters in α-, β- and γ-CyD at 2 K are shown in Fig. 2 with thick solid curves. The absorption spectra were derived by eq. (1). The lowest absorption peak energies are at around 5 eV. These absorption bands are not clearly separated. The absorption bands overlap with other absorption which are the tails extending from higher energy area. For the first step, the tail part was subtracted from the spectrum by postulating the Gaussian shape. The rest of the absorption spectrum does not show a single Gaussian shape. It is reasonable to speculate that the absorption band is made of two absorption bands separated by the spin–orbit splitting. The best fit has been done using two Gaussian functions. The three bands analysis fits well to the observed absorption band shown with thick solid line in Fig. 2. The separation of the low energy pairs of absorption bands are 0.72 eV (α-CyD), 0.68 eV (β-CyD) and 0.63 eV (γ-CyD). These values are nearly the same but a small amount larger than the spin–orbit splits observed in the single crystal which are shown in Fig. 1. The intensity ratio of the pair absorption at 4.47 eV and 5.10 eV is not equal to 2 : 1 according to the multiplicity ratio of bromine. Absorption spectra of 77 K and RT are shown in Figs. 3 and 4, respectively. The spin–orbit split pairs are analyzed and shown with broken lines. Their split energies range from 0.42 eV to 0.72 eV.

The first absorption peak energy shifts from 4.56 eV (2 K) to 4.95 eV (RT), 4.83 eV (2 K) to 4.73 eV (RT) and 4.47 eV (2 K) to 4.67 eV (RT) in α, β and γ-CyD, respectively. The peak energy shift between RT and 2 K are 0.39 eV, 0.10 eV and 0.20 eV in α, β and γ-CyD, respectively. On the other hand, the peak energy shifts from 3.64 eV to 4.47 eV between the single crystal and cluster at 2 K as shown in Fig. 5. The shift energy is 0.83 eV.

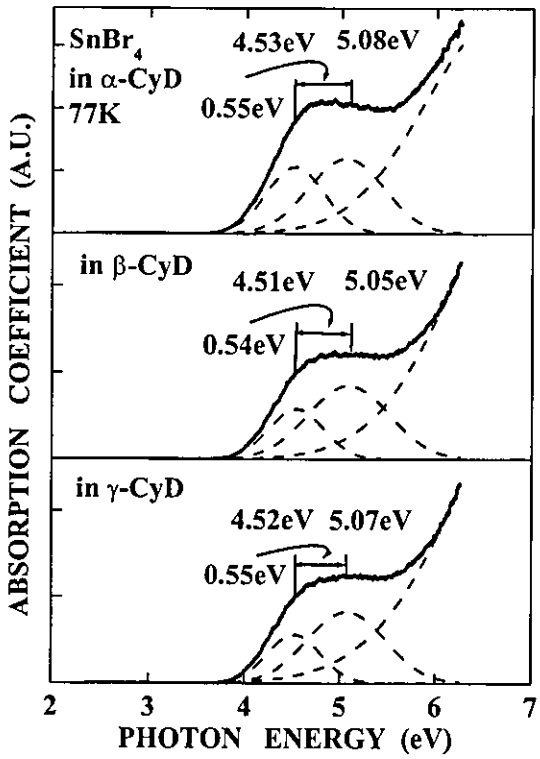

Fig. 3. Absorption spectra of $SnBr_4$ cluster in α-, β- and γ-cyclodextrins at 77 K. These spectra were derived from the reflection spectra of powder sample by using Kubelka–Munk formula.

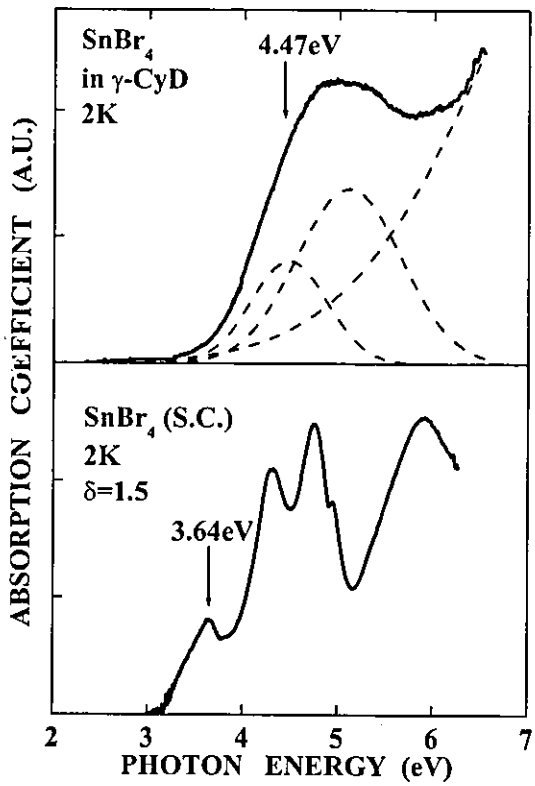

Fig. 5. Comparison of the absorption spectra between $SnBr_4$ single crystal and its cluster in γ-cyclodextrins at 2 K, which are shown in Figs. 1 and 2.

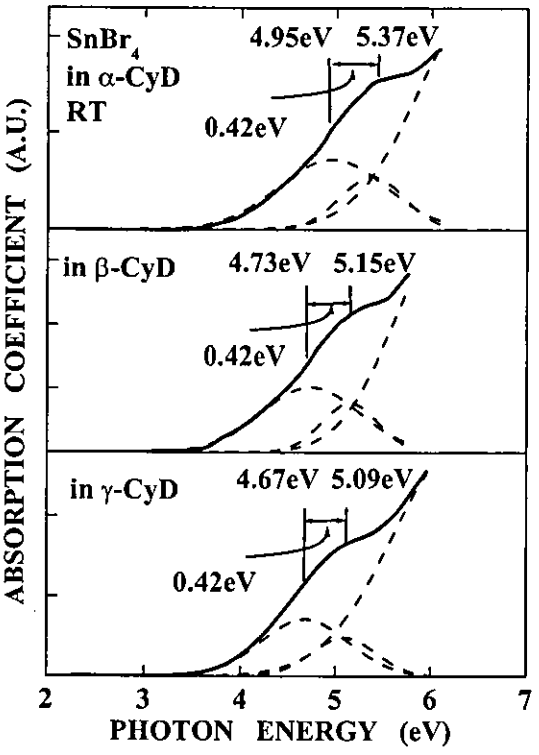

Fig. 4. Absorption spectra of $SnBr_4$ cluster in α-, β- and γ-cyclodextrins at room temperature. These spectra were derived from the reflection spectra of powder sample by using Kubelka–Munk formula.

3. Discussion

Transition energies from HOMO to LUMO of $SnBr_4$ single molecule are in the range between 4.5 eV and 5.5 eV as seen in Figs. 2–4. The exciton energies in the single crystal are in the range between 3.21 eV (RT) and 3.64 eV (2 K) as shown in Fig. 1. The large peak energy shift shows the quantum size effect. In Figs. 2–4, spin–orbit pair of absorption bands was not observed separately, because each band width is wide and the separation is small. The coupling between electrons and molecular vibrations is stronger than that in a SnI_4 molecule, because $SnBr_4$ has more ionic character than SnI_4 and thus electron interacts more strongly with molecular vibrations in $SnBr_4$ than in SnI_4. The spin–orbit coupling strength is smaller in a $SnBr_4$ than that in a SnI_4. These relative intensities are reasonable because the larger atomic number atom has stronger spin–orbit coupling.

In the previous paper, we reported on the optical spectra of SnI_4 cluster. There are two separated absorption bands. Their energy separation is 0.8 eV and they were assigned as the split pairs of spin–orbit coupling. The purpose of the present work is to know the electric energy states and to assure the pair absorption bands comes from the spin–orbit interaction. In the present work we assured the spin–orbit splitting by dividing the broad absorption bands into two bands which are separated by the spin–orbit splits between 0.42 eV and 0.72 eV and are in the reasonable energy region.

It is estimated by considering the sizes of CyD's that $SnBr_4$ molecules are inserted two, three and five into α-, β- and γ-CyD, respectively. The lowest energy peaks of these spin–orbit split pairs have no relation to the sizes of α-, β- and γ-CyD, that is, the peak energies do not depend on the cluster sizes. This result means that the $SnBr_4$ molecules inside a CyD are almost independent and they do not interact each other so strongly as to change their energy levels. In fact, there are very large ambiguities to decide these peak

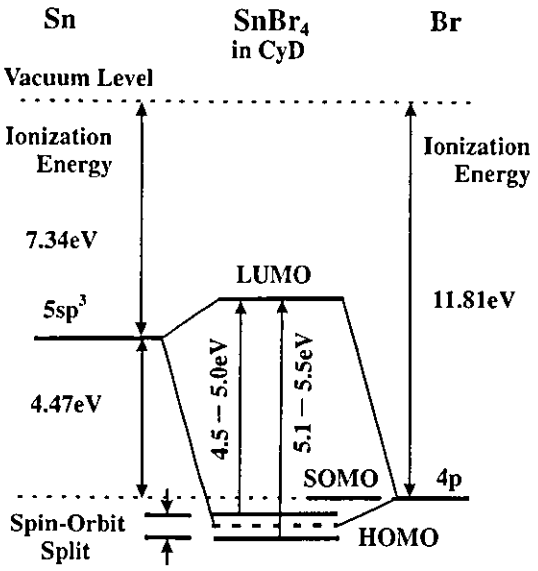

Fig. 6. Proposed molecular orbital energy levels of $SnBr_4$ molecule.

energies when we analyzed the absorption bands. It is also the same for the intensity ratios of these spin–orbit split pairs that we could not deduce out the exact intensity ratio, 2 : 1. There is another reason why the ratio is not 2 : 1 in $SnBr_4$. The bonding is covalent between a tin and four bromines. If the bonding is ionic and the tin is a cation, Sn^{4+} and bromine is an anion, Br^-, then the electron configuration of Br^- is the same as the closed shell of the Kr, and the spin–orbit coupling splits the $4p^6$ level to a quartet and a doublet. The transition from these levels to the 5s level of Sn^{4+} will show the absorption intensity ratio of 2 : 1. In fact, the real bonding in $SnBr_4$ is covalent and the electron states of the tin and the four bromines are mixed. Therefore, the absorption spectra do not show the exact 2 : 1 ratio.

We propose the energy diagram of $SnBr_4$ molecule as shown in Fig. 6. The ground state of the $SnBr_4$ is the covalent bonding state between the bromine $4p_z$ and the tin sp^3 hybrid orbitals. The directions of z are those from each bromine to the central atom of tin. The lowest unoccupied molecular orbital (LUMO) which is composed of the anti-bonding orbital of the same bromine $4p_z$ and the tin sp^3-mixing states. The lowest excitation is the intramolecular excitation from the bonding HOMO state to the anti-bonding LUMO state. The LUMO state is anti-bonding state and easily decomposes, thus the emission from this level will not occur. We could not observe any emission. There is another non-bonding state (SOMO). It is a slightly higher energy state than the bonding state. The transition from this SOMO state to the LUMO state is forbidden, because the wave-functions of iodine $4p_x$ and $4p_y$ spread at right angle to those of the LUMO, and thus there is no overlapping between these wavefunctions.

The energy levels of bromine 4p is 11.81 eV lower than the vacuum level, which is estimated from the ionization energy of the Br atom. In addition, it is lower than that by loosing the energy for the binding energy, when bromine atoms form a $SnBr_4$ molecule. Taking into account this energy decrease, the HOMO state is expressed with thick broken line below. The HOMO state splits to two levels by spin–orbit interaction. The LUMO state is mainly formed from $5sp^3$ state of tin. The $5sp^3$ energy level is 7.34 eV lower than the vacuum level. It would increase the energy a little by forming an anti-bonding LUMO state. The energy difference between HOMO and LUMO is larger than 4.47 eV which is the energy difference between 4p state of bromine and $5sp^3$ state of tin. The observed absorption peak energies are between 4.5 eV and 5.0 eV for the lowest absorption and between 5.1 eV and 5.5 eV for the second absorption bands. They are quite close to the estimated energy of 4.47 eV. This indicates that the present energy level assignment is correct, and thus it is assured that the previously reported absorption bands in SnI_4 are also consistent.

Acknowledgements

We would like to thank to Mr. M. Saito of Tohoku University for his technical assistance. This work has been carried out under the support of Grant-in-Aid for Scientific Research from the Japanese Ministry of Education, Culture, Sports, Science and Technology (No. 13874037). We would like to thank Mr. M. Moriya, the Chairman of Seiki Group Companies for the support of research fund. We also thank to Mr. S. Furusawa for producing the coolant of liquid nitrogen.

1) M. L. Bender and M. Komiyama: *Cyclodextrin Chemistry* (Springer-Verlag, Tokyo, 1978).
2) T. Yoshinari, A. Ohnishi, T. Yamada, T. Shigihara, M. Omaru, T. Kamikawa and T. Goto: Mater. Sci. Eng. **217/218** (1996) 119.
3) M. Omaru, S. Takahashi, A. Ohnishi, T. Yoshinari, S. Nagasaka, T. Kamikawa and T. Goto: J. Phys. Soc. Jpn. **66** (1997) 1816.
4) H. Reuter and R. Pawlak: Z. Anorg. Allg. Chem. **626** (2000) 925.
5) H. Reuter and R. Pawlak: Z. Kristallogr. **216** (2001) 34.
6) G. R. Hearne, M. P. Pasternak and R. D. Taylor: Phys. Rev. **52** (1995) 9209.
7) J. M. Hossenlopp, F. J. Lamelas, K. Middleton, J. A. Rzepiela, J. D. Schmidt and A. Zivkovic: Appl. Organomet. Chem. **12** (1998) 147.
8) R. Belosludov, T. Yoshinari, T. Hiwada, Y. Kawazoe, K. Ohno and S. Nagasaka: *Clusters and Nanomaterials*, ed. Y. Kawazoe, T. Kondow and K. Ohno (Springer-Verlag, 2001) Springer Series in Cluster Physics, Chap. 5, pp. 109–131.
9) P. Kubelka and F. Munk: Z. Tech. Phys. **12** (1931) 593.

First-principles study of the electronic structures of icosahedral Ti_N (N=13,19,43,55) clusters

Shan-Ying Wang[a)]
Institute for Materials Research, Tohoku University, Aoba-ku, Sendai 980-8577, Japan and Department of Physics, Tsinghua University, Beijing 100084, China

Jing-Zhi Yu and Hiroshi Mizuseki
Institute for Materials Research, Tohoku University, Aoba-ku, Sendai 980-8577, Japan

Jia-An Yan
Department of Physics, Tsinghua University, Beijing 100084, China

Yoshiyuki Kawazoe
Institute for Materials Research, Tohoku University, Aoba-ku, Sendai 980-8577, Japan

Chong-Yu Wang
Department of Physics, Tsinghua University, Beijing 100084, China and Center Iron and Steel Research Institute, Beijing 100081, China

(Received 29 December 2003; accepted 20 February 2004)

We have studied the electronic structures of icosahedral Ti_N clusters (N=13, 19, 43, and 55) by using a real-space first-principles cluster method with generalized gradient approximation for exchange-correlation potential. The hexagonal close-packed and fcc close-packed clusters have been studied additionally for comparisons. It is found that the icosahedral structures are the most stable ones except for Ti_{43}, where fcc close-packed structure is favorable in energy. We present and discuss the variation of bond length, the features of the highest occupied molecular orbitals and the lowest unoccupied molecular orbital, the evolution of density of states, and the magnetic moment in detail. The results are in good agreement with the predictions from the collision-induced dissociation and size-selected anion photoelectron spectroscopy experiments. © *2004 American Institute of Physics.* [DOI: 10.1063/1.1701769]

I. INTRODUCTION

Transition-metal clusters have received much scientific and technological interest and been widely studied in the recent two decades.[1] They show the distinction of complexity in both geometrical structure and magnetism. The localized and unfilled d shells usually result in spin multiplets and low-lying energy states that bring many useful physical and chemical properties for transition-metal clusters, making them highly promising in nanotechnological applications.

The evolution of electronic structure from atoms to the bulk is an important question, involving the evolutions of bond length, density of states (DOS), magnetic moment, and the energy gap between the highest occupied molecular orbital (HOMO) and the lowest unoccupied molecular orbital (LUMO). The clusters of medium size consisting of tens to several tens atoms are particularly important in the research. To our knowledge, clusters composed of the later part of $3d$ elements such as Mn, Fe, Co, and Ni have been widely studied.[2–9] For medium-size V, Ti, and Cr clusters, the geometrical structure, electronic structure, and magnetism are still unknown even though they are believed to be simple and expected to show some bulk features. Size-selected anion photoelectron spectroscopy (PES) is powerful experimental technique for exploring the electronic structure of clusters, with which Wang's group has obtained many valuable and meaningful results on transition-metal clusters.[10–15] Their experiments on Ti clusters[10,11] have shown that the pronounced narrowing of PES features occurs for Ti_{13}^- and Ti_{55}^-, and the $3d$ band emerges at the eight-atom cluster, beyond which the d band broadens and evolves toward that of the bulk. These and another collision-induced dissociation experiment[16] suggest that Ti_{13}, Ti_{19}, and Ti_{55} clusters prefer an icosahedral structure. More recently, Castro *et al.* also reported their first-principles study of the ultrafine Ti_N and Ti_N^{-1} (N=3–8,13) clusters,[17] where the theoretical results are in good agreement with their experimental results. In the previous study of icosahedral Ti_{13} clusters,[18] we found that the bonding feature in the cluster is close to that in the hexagonal bulk Ti obtained by energy band calculations.[19] However, the characteristic bond lengths (2.57 and 2.70 Å) are much shorter than that (2.95 Å) of bulk Ti.

Actually it is still difficult to detect only by experimental approaches the exact geometrical structure of clusters. Nevertheless, associating with the experimental measurements, scientists can predict effectively and accurately some unknown structures by employing the first-principles method based on density functional theory (DFT).[20,21] In the present work, we study the electronic structure of icosahedral (ico) Ti_N clusters (N=13, 19, 43, and 55) by using a real-space first-principles cluster method named density functional for molecules (DMol).[22,23] Bulk Ti shows the hexagonal close-

a)Electronic mail: sywang@imr.edu

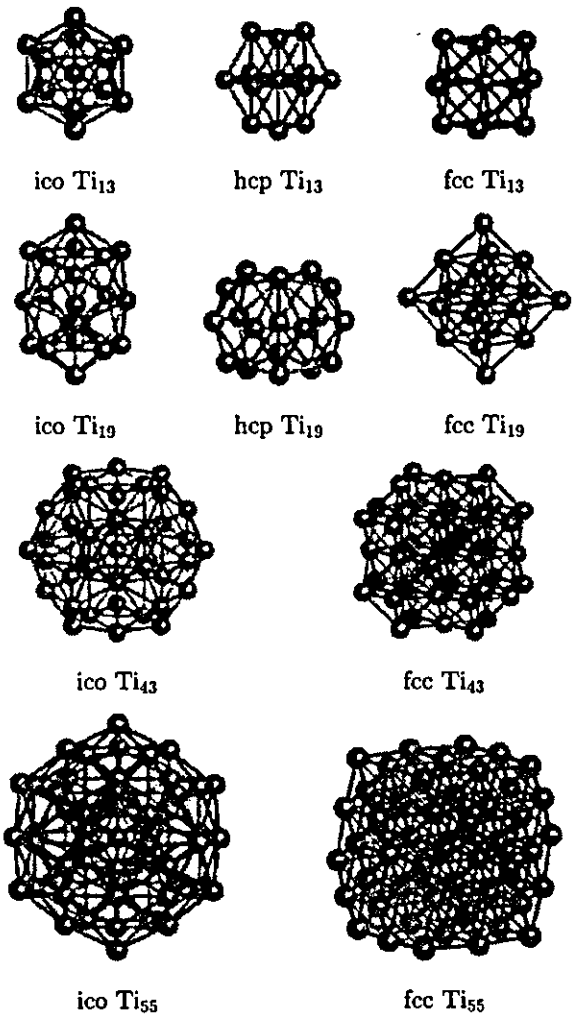

FIG. 1. The ico, hcp, and fcc structures of Ti clusters.

packed (hcp) instead of the fcc close-packed (fcc) phase at low temperature. For comparison, the studies of the hcp structures of Ti_{13} and Ti_{19} and the fcc structures of Ti_{13}, Ti_{19}, Ti_{43}, and Ti_{55} are included. We present and discuss the binding energy, bond length, HOMO and LUMO states, DOS, and magnetism in detail.

II. METHOD AND COMPUTATIONAL DETAILS

DMol is a widely used real-space first-principles cluster method based on DFT and has been applied to many problems on molecular clusters, chemisorption, surface reconstruction, and the ground state of highly correlated transition-metal clusters. It performs accurate and efficient self-consistent calculations and structural optimization by using, respectively, a fast-convergent three-dimensional numerical integration scheme and several effective local-minimum searching techniques. The equilibrium structure and total energy can be obtained by relaxing atoms until the forces are deemed to be zero.

In first-principles calculations, one must minimize as far as possible the effects of the basis and the exchange-correlation functional on the results. The inner orbitals such as $3s$ and $3p$ sometimes are important for the ground-state properties of transition metals. This is particularly true for ultrafine Ti clusters.[24] We choose a double-numerical basis with polarized functions and only froze the $1s2s2p$ orbitals in the calculations. The general gradient approximation (GGA) is used by combining the correlation functional of Perdew[25] with exchange functional of Becke.[26] All calculations are spin unrestricted. The parameters used here were tested by Ti_2 dimes.[18] For accurate calculations, we choose an octuple scheme for the multipolar fitting procedure (the maximum angular momentum of the fitting function is set to be 3) on the charge density and Coulomb potential and a fine grid scheme for numerical integration (about 1500 integration points per atom). In the optimizations, the energy gradient and atomic displacement are converged to 0.03 eV $Å^{-1}$ and 5×10^{-4} Å, respectively. The charge density in the self-consistent iterations is converged to 1×10^{-5}, which allows a total energy convergence of 1×10^{-4} eV. The binding energy (BE) is defined as

$$\mathrm{BE}=E_a-E_t,$$

where E_a is the sum of the total energies of all single atoms and E_t is the total energy of the cluster.

Figure 1 shows the geometrical structures of the clusters. All the hcp and fcc structures are generated originally from the bulk state according to the neighboring relationship. The ico Ti_{43} cluster is generated by adding 30 atoms on top of edge positions of the ico Ti_{13} cluster and ico Ti_{55} cluster by adding additional 12 atoms on top of vertex positions. In structural optimizations, all atoms are relaxed freely under a symmetrical restriction—i.e., holding I_h, O_h, and D_{3h} symmetries for Ti_{13} and Ti_{19} clusters and D_{5d} and O_h symmetries for Ti_{43} and Ti_{55} clusters. For a technical reason from the DMol executive code, we have to use subgroup D_{5d} instead of I_h to reduce the Hamiltonian matrix in the calculation for ico Ti_{43} and Ti_{55} clusters. This can be taken as a very weak Jahn–Teller effect and has little effect on the discussion, since the energy levels near the Fermi level show much slight splitting (not beyond 0.006 eV, nearly degenerate states) and those bonds that are equivalent at I_h symmetry show little difference in length (usually not beyond 1% except for only two bonds change by about 3% in Ti_{43}). For an easy discussion, we will use the averaged quantities (bond length and atomic magnetic moment) for those atoms that are equivalent at I_h symmetry.

TABLE I. Calculated binding energies in eV for the ico, hcp, and fcc structures. The binding energy per atom is included in the parentheses.

	Ti_{13}	Ti_{19}	Ti_{43}	Ti_{55}
ico	54.20(4.17)	82.81(4.36)	188.52(4.38)	259.43(4.72)
hcp	51.48(3.96)	80.83(4.25)		
fcc	50.77(3.91)	77.17(4.06)	194.34(4.52)	255.88(4.65)

III. RESULT AND DISCUSSION

All data on ico Ti_{13} cluster listed in Tables I–IV are quoted from our previous work.[18]

TABLE II. Calculated bond lengths in Å and the corresponding bond numbers in the ico, hcp, and fcc structures. The averaged bond length and total number of effective bonds of cluster are also given. l_{ij} denotes the length of the bond formed by atoms in the ith and jth shells with respect to the center of cluster (atom at the center is indexed by the zeroth shell except for icosahedral Ti_{19} cluster, where the two inner atoms are indexed by the zeroth shell). The bonds are counted within an 2.95 Å cutoff in length (a characteristic bond length of bulk Ti). For Ti_{43} and Ti_{55}, l_{02}, l_{03}, and l_{04} are given additionally for showing the radii of the shells.

	Ti_{13}			Ti_{19}			Ti_{43}			Ti_{55}	
ico	l_{01}	2.567,12	ico	l_{00}	2.324,1	ico	l_{01}	2.754,12	ico	l_{01}	2.720,12
	l_{11}	2.699,30		l_{01}	2.464,2		l_{11}	2.896,30		l_{11}	2.867,30
					2.545,10		l_{12}	2.614,60		l_{12}	2.722,60
hcp	l_{01}	2.585,6			2.811,10		l_{22}	2.793,60		l_{13}	2.436,12
		2.680,6		l_{11}	2.684,10		l_{02}	4.519,30		l_{22}	2.864,60
	l_{11}	2.518,3			2.707,10					l_{23}	2.723,60
		2.613,6			2.714,20	fcc	l_{01}	2.819,12		l_{02}	4.634,30
		2.651,3					l_{11}	2.819,24		l_{03}	5.159,12
		2.656,12	hcp	l_{01}	2.799,6		l_{12}	2.698,24			
				l_{11}	2.284,3		l_{13}	2.659,48	fcc	l_{01}	2.760,12
fcc	l_{01}	2.648,12			2.725,12		l_{23}	2.730,24		l_{11}	2.760,24
	l_{11}	2.648,24			2.943,6		l_{33}	2.673,24		l_{12}	2.750,24
				l_{12}	2.470,12		l_{02}	3.811,6		l_{13}	2.765,48
					2.527,12		l_{03}	4.696,24		l_{14}	2.622,12
										l_{23}	2.793,24
			fcc	l_{01}	2.754,12					l_{33}	2.704,24
				l_{11}	2.754,24					l_{34}	2.694,48
				l_{12}	2.656,24					l_{02}	3.889,6
										l_{03}	4.786,24
										l_{04}	5.382,12
ico	2.661,42			2.683,63			2.743,162			2.762,234	
hcp	2.629,36			2.627,51							
fcc	2.648,36			2.715,60			2.715,156			2.735,216	

A. Binding energy

The calculated BEs are listed in Table I. For the Ti_{13} cluster, the ico structure is the lowest-energy state and the BE is 54.20 eV, larger than those of hcp and fcc structures by about 2.72 and 3.43 eV, respectively. Similarly, the ico Ti_{19} shows the highest BE 82.81 eV, about 1.98 and 5.64 eV larger than those of hcp and fcc structures, respectively. For Ti_{43}, however, the fcc structure becomes the lower-energy state and the BE is 194.34 eV, about 5.82 eV larger than that of ico structure. For Ti_{55}, the ico structure has again the higher BE 259.43 eV, about 4.55 eV larger than that of fcc structure. These results suggest that the ico Ti_{13}, Ti_{19}, and Ti_{55} and the fcc Ti_{43} clusters are favorable in energy, which are in agreement with the predictions from the size-selected anion PES and the collision-induced dissociation experiments.[10,11,16] In fact, no evidence has been found in the PES experiments that the Ti_{43} cluster will prefer an ico structure. On the contrary, the PES experiments support a tentative conclusion that the medium-size Ti clusters may possess bcc-type structure since the medium-size anion Ti clusters show similar two-band features in PES spectra as anion V clusters. The cluster packing for the medium-size Ti cluster is very complicated and needs further investigation from both experiment and theoretical calculations. Table I also gives the calculated BE per atom. For those structures favorable in energy, the BE per atom increases smoothly from Ti_{13} to Ti_{55} (4.17, 4.36, 4.52, and 4.72 eV) and can be expected to approach the cohesive energy of bulk Ti (4.85 eV per atom) for larger Ti clusters.

B. Bond length

Table II gives the results of the calculated bond lengths (BLs) and the bond numbers in the ico, hcp, and fcc structures. The bonds are counted by a reasonable cutoff 2.95 Å (a characteristic bond length of bulk Ti), within which the interaction between the two atoms are believed to be effective. We call these bonds as effective bonds (EBs). We classify all atoms by shells according to their neighboring relationship with respect to the center of the cluster (the atom at the center is indexed by the zeroth shell). Note that for ico Ti_{19} (it is indeed a bi-icosahedral structures), since there is no atom at its center, we simply group the 19 atoms into two shells and index the two inner atoms (refer to Fig. 1) by the zeroth shell. All bonds are denoted by the shell index in Table II.

We first discuss the BL variations in the *ico structure*. For Ti_{19}, the two inner atoms have the shortest BL (l_{00} = 2.324 Å), which implies a strong interaction between them. Comparing with Ti_{13}, the two BLs l_{01} in the main symmetry axis decrease to a rather short value 2.464 Å. Most of the BLs (l_{11}) in the first shell increase. The results indicate that the bi-icosahedral structure of Ti_{19} shrinks along its main symmetry axis, but expands transversely compared with Ti_{13}. For Ti_{43}, we can see an interesting phenomenon that the second shell makes the first shell expand. Compared with Ti_{13} and Ti_{19}, the l_{01} and l_{11} keep on increasing and those EBs within the first shell are weakened. The l_{22} takes a relatively large value 2.793 Å while the l_{12} shows a relatively short value 2.614 Å, indicating that the EBs (l_{12}) be-

TABLE III. Calculated HOMO and LUMO states in the ico, hcp, and fcc structures. The symbols "+" and "−" denote the spin-up and spin-down states, respectively. E denotes the energy in eV and n denotes the electron occupation number.

	ico			hcp			fcc		
	State	E	n	State	E	n	State	E	n
Ti_{13}	T1U(−)	−3.886	2	$E'(-)$	−3.588	1	T2U(±)	−3.369	6
	HG(−)	−3.741	0	$A2'(-)$	−3.454	0	T1U(±)	−3.213	0
Ti_{19}	$E1''(+)$	−3.961	2	$E''(\pm)$	−3.807	2	T2U(+)	−3.793	3
	$E1''(-)$	−3.846	0	$A2'(\pm)$	−3.736	0	A2U(+)	−3.772	0
Ti_{43}	A1G(−)	−3.596	1				T2G(−)	−3.586	2
	A2U(−)	−3.563	0				A1G(+)	−3.578	0
Ti_{55}	E2G(±)	−4.279	4				T1G(+)	−3.899	3
	A1U(±)	−4.114	0				T1U(+)	−3.887	0

tween the first and second shells become more important for the binding property of Ti_{43}. For Ti_{55}, due to the presence of the third shell, the first shell is contracted and the second shell expands somewhat compared to those of Ti_{43}. Consequently, the l_{11} decreases while the l_{12} and l_{22} increases. The BLs between the neighboring different shells (l_{01}, l_{12}, and l_{23}) in Ti_{55} show little difference (not beyond 0.003 Å) and reach basically to an equilibrium state. Surprisingly, the first shell still has 12 strong EBs (l_{13}=2.436 Å) with the third shell in Ti_{55}. For all ico structures, it can be found that the EBs between the different shells (l_{01}, l_{12}, l_{13}, and l_{23}) are shorter than those in the same shell (l_{11} and l_{22}) except for the 11 EBs (l_{00}=2.324 Å, l_{01}=2.811 Å) in the bi-icosahedral structure of Ti_{19}. It seems that the interactions between the different shells are more important than those in the same shells for the binding property of medium-size ico Ti clusters.

Now we discuss the case in the *hcp and fcc structures*. For hcp Ti_{13}, the l_{01} increases and l_{11} reduces to some extent compared with those in the ico structure. For hcp Ti_{19}, all EBs within the first shell expand remarkably compared with those in Ti_{13} except for the three EBs in the hexagonal ring, which, however, decrease greatly (l_{11}=2.284 Å) and become the strongest. Note the other three EBs in the hexagonal ring are destroyed: the 24 EBs (l_{11}) in Ti_{13} decrease to the 21 EBs in Ti_{19}. The EBs between the first and second shells in hcp Ti_{19} are much stronger since they show relatively short values in length (l_{12}=2.470,2.527 Å). For all fcc structures, it is interesting that the BLs between the center atom and the atoms in the first shell are equal to those between the atoms in the first shell ($l_{01}=l_{11}$). The variation features of EB from fcc Ti_{13} to Ti_{55} are similar to the case of ico structures. From fcc Ti_{13} to Ti_{43}, the BLs l_{01}, l_{11}, and l_{12} increase continuously, indicating the expanding of the first and second shells. Compared with fcc Ti_{43}, the first shell in fcc Ti_{55} shrinks somewhat while the second shell expands largely.

It can be seen that the ico structure has more EBs than the hcp and fcc structures. However, the averaged BL of ico structure is not the shortest. It seems that the binding energy is not directly or explicitly related to these quantities.

C. HOMO and LUMO states

Table III presents data on the HOMO and LUMO states. For ico clusters, the HOMO–LUMO gaps are comparatively large, beyond 0.14 eV, with the exception of a much small value ~0.03 eV for Ti_{43}. All the ico clusters are spin polarized except for Ti_{55}, which has fully paired electrons and becomes a closed-shell system. The ico Ti_{19} is a semifilled open-shell system while Ti_{13} and Ti_{43} have additional unpaired electrons in molecular orbitals besides the HOMO. For hcp clusters, Ti_{13} is an open-shell system with a comparatively large HOMO–LUMO gap ~0.13 eV and Ti_{19} is a closed-shell system with a small one ~0.07 eV. For fcc clusters, Ti_{13} is a closed-shell system, and Ti_{43} and Ti_{55} show near-zero HOMO–LUMO gaps.

D. Density of states and magnetism

The size-selected anion PES experiments[10,11] have shown that the $3d$ band emerges at the eight-atom Ti cluster, and broadens and evolves toward the bulk characteristics with the increase of cluster size. In order to well understand the phenomena observed in the experiment, we present the total DOS and spin-dependent total DOS of ico Ti_{13}, Ti_{19}, Ti_{55}, and fcc Ti_{43} clusters in Figs. 2 and 3, respectively. The total DOS is calculated by broadening the energy levels ε_i of molecular orbitals by using a line-shape function Lorentzian with width δ=0.1 eV as follows:

$$\mathrm{DOS}(E)=\sum_i \frac{\delta/\pi}{(E-\varepsilon_i)^2+\delta^2}.$$

Two significant resonant peaks A and B as shown in Fig. 2 can be identified from the onset of DOS of valent states, which are both $s,p-d$ hybridizations states. With the increasing of cluster size, the two peaks decompose somewhat and become more structurized, and the site difference between their spectral centers decreases from about 2.5 to 1.5 eV by a rough evaluation. These results are basically in agreement with the PES experiment, where a two-band structure with a site difference of about 1.5 eV was observed for medium-size Ti clusters. For PES, it is not surprising that there are differences between the experiment and first-principles calculation, since the DFT used in most of the first-principles methods is still a ground-state theory. However, PES is involved in very complicated electronic exciting process.

There are several features displaying how the DOS evolves from Ti_{13} to Ti_{55}. First, a little peak of $4s$ states

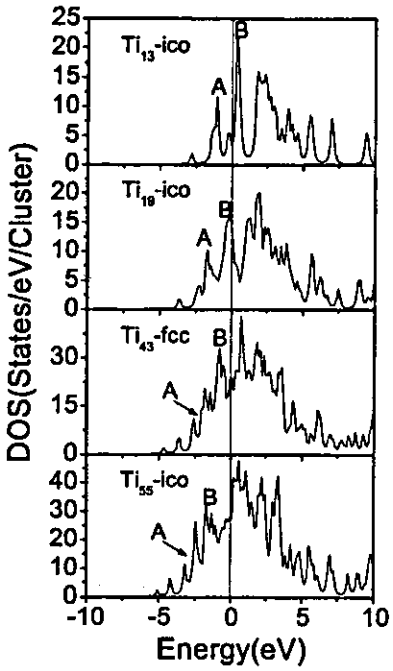

FIG. 2. The total DOS of the ico Ti_{13}, Ti_{19}, Ti_{55}, and fcc Ti_{43} clusters. The Fermi level is shifted to zero.

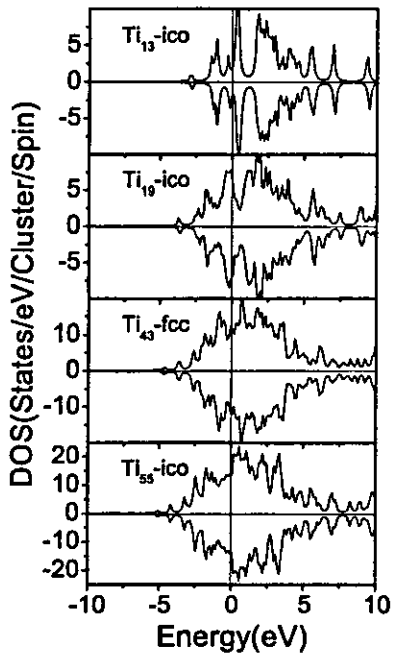

FIG. 3. The spin-dependent total DOS of the ico Ti_{13}, Ti_{19}, Ti_{55}, and fcc Ti_{43} clusters. The spin-up and spin-down states are displayed in the up panel (plus value) and down panel (minus value), respectively. The Fermi level is shifted to zero.

appearing at the initial position of DOS curve shifts to the lower-energy positions and the peak value reduces successively from Ti_{13} to Ti_{55}. Next, there is a remarkably deep valley around 1.2 eV in Ti_{13}, which dwindles largely in size in Ti_{19} and disappears in Ti_{43} and Ti_{55}. Then, closely associating with the above two features, the DOS spreads out to a relatively wide energy range from Ti_{13} to Ti_{55}. Finally, we can notice that the appearance of the total DOS of Ti_{55} is very close to that of bulk Ti.[19,27] Particularly, the DOS that locate within the energy range crossing the Fermi level from about -2.2 to 2.2 eV show similar variation characteristics as the bulk Ti: a large extended peak followed by an ascent crossing the Fermi level, and then comes another large extended peak. One can expect that the features of the DOS of bulk Ti will be present more completely in larger clusters than Ti_{55}. It may be reasonable to take approximately the above features as the DOS evolution from cluster to bulk.

On the other hand, unlike other transition-metal clusters, these medium-size Ti clusters show complex $s,p-d$ hybridization states rather than distinct $3d$ localized characteristics. We can see that the hybridization states span a relatively wide energy range. These features actually are closely related to the electronic configuration of the Ti atom. Due to the fewer electrons occupying $3d$ orbitals, the Ti atom has relatively expanded $3d$ states in space compared to the latter part of $3d$ elements like Fe, Co, and Ni. These $3d$ states are easily delocalized by $s,p-d$ hybridizations, which appears to result in a weak magnetism for Ti clusters. It can be seen from Fig. 3 that the ico Ti_{13} and Ti_{19} and the fcc Ti_{43} clusters show just slight exchange splittings and possess total magnetic moments of $(6.0,2.0,4.0)\mu_B$, respectively (see Table IV). The ico Ti_{55} is nonmagnetic and there is no exchange splitting in total DOS. For Ti_{13}, the state of $0.0\mu_B$ is about 0.61 eV higher than the ground state of $6.0\mu_B$. Castro *et al.* have reported a ground state of $0.0\mu_B$ (closed shell state) with the state of $2.0\mu_B \sim 0.03$ eV higher.[17] This discrepancy mainly comes from the differences for treating spin and symmetry. We obtained the states of $6.0\mu_B$ $(0.0\mu_B)$ by using a pure spin-polarized (spin-unpolarized) mode instead of a constraint on the total-spin state of the cluster (singlet and triplet) as used by Castro *et al.* Nevertheless, both ways can yield a reasonable description of the magnetism of transition-metal clusters and further experiments on the magnetism of Ti clusters is necessary for examination. On the other hand, we used an I_h symmetry constraint in the structural optimi-

TABLE IV. Calculated atomic magnetic moments in μ_B in ico Ti_{13}, Ti_{19}, and Ti_{55} and fcc Ti_{43} clusters. The total magnetic moment of cluster is also given either. The numbers 0, 1, 2, and 3 index the atomic shells with respect to the center of cluster (atom at the center is indexed by the zeroth shell except for icosahedral Ti_{19} cluster, where the two inner atoms are indexed by the zeroth shell).

	0	1	2	3	Total
Ti_{13} (ico)	0.202	0.483			6.000
Ti_{19} (ico)	−0.054	0.124			2.000
Ti_{43} (fcc)	0.169	−0.010	0.209	0.112	4.000
Ti_{55} (ico)	0.000	0.000	0.000	0.000	0.000

zation and Castro *et al.* did without symmetry—i.e., full optimization. It should be pointed out that as a result of spin polarization, even for the deeper occupied molecular orbitals, its spin-up and spin-down states can be nondegenerate. The total magnetic moment of clusters is determined by the difference between the electron numbers in the spin-up and spin-down molecular orbitals. Thus we can see from Tables III and IV that Ti_{13} has a total magnetic moment of $6.0\mu_B$; i.e., there are totally six unpaired spin-up electrons, while there are two spin-down electrons in its HOMO. The center atom of ico Ti_{13} forms spin ferromagnetic states with its 12 neighboring atoms, whereas the inner two atoms of ico Ti_{19} form spin antiferromagnetic states with the outside atoms. For fcc Ti_{43}, the atomic magnetic moments in the first shell are antiparallel with all others in the cluster. The atomic magnetic moments in ico Ti_{55}, however, are completely quenched. Usually, the enhanced local magnetic moments are expected to appear in the low-dimensional systems of transition-metal-like clusters, surfaces, and interfaces, where the lower symmetry and coordination number are two favorable factors for magnetism. Such a property, however, seems not extend to Ti since these medium-size clusters just show very weak magnetism compared to nonmagnetic bulk Ti.

IV. CONCLUSION

The first-principles DMol method based on DFT with the GGA is employed for studying the electronic structures of the icosahedral, hexagonal close-packed, and fcc close-packed Ti_N clusters ($N=13$, 19, 43, and 55). For all these medium-size clusters, the icosahedral structures are found to be favorable in energy except for Ti_{43}, where the fcc close-packed structure is the lower-energy state. With the increase of cluster size, the atomic shells show complex expanding or shrinking behaviors. The bonding between the different atomic shells is more important for the binding property of icosahedral structure. The icosahedral structure has more effective bonds and a longer averaged bond length than the hexagonal close-packed and fcc close-packed structures. The icosahedral Ti_{13} and fcc close-packed Ti_{43} are open-shell systems with additional unpaired electrons in molecular orbitals besides the HOMO. The icosahedral Ti_{19} and Ti_{55} are, respectively, a semifilled open-shell system and closed-shell system, and the latter has the largest HOMO–LUMO gap ~0.17 eV. The total DOS, particularly those states near the Fermi level of icosahedral Ti_{55}, are very close to that of bulk Ti. The variation of the DOS from Ti_{13} to Ti_{55} indicates approximately the DOS evolution from cluster to bulk. All clusters show strong $s,p-d$ hybridization states, which result in a very weak magnetism of icosahedral Ti_{13}, Ti_{19}, and fcc close-packed Ti_{43} and quenched atomic magnetic moments in icosahedral Ti_{55}. The results are in agreement with the predictions from the collision-induced dissociation and size-selected anion photoelectron spectroscopy experiments.

ACKNOWLEDGMENTS

We thank the crew of the Center for Computational Materials Science (CCMS) of the Institute for Materials Research (IMR), Tohoku University, Japan, for their support of computing facilities. This work was partially supported by "973" Project from the Ministry of Science and Technology of the People's Republic of China (Grant No. G2000067102).

[1] J. A. Alonso, Chem. Rev. **100**, 637 (2000).
[2] Z. Q. Li and B. L. Gu, Phys. Rev. B **47**, 13611 (1993).
[3] F. A. Reuse and S. N. Khanna, Chem. Phys. Lett. **234**, 77 (1995).
[4] F. A. Reuse, S. N. Khanna, and S. Bernel, Phys. Rev. B **52**, R11650 (1995).
[5] P. Ballone and R. O. Jones, Chem. Phys. Lett. **233**, 632 (1995).
[6] N. N. Lathiotakis, A. N. Andriotis, M. Menon, and J. Connolly, J. Chem. Phys. **104**, 992 (1996).
[7] M. Castro, Int. J. Quantum Chem. **64**, 223 (1997).
[8] Tina M. Briere, Marcel H. F. Sluiter, V. Kumar, and Y. Kawazoe, Mater. Trans., JIM **43**, 424 (2002).
[9] Tina M. Briere, Marcel H. F. Sluiter, V. Kumar, and Y. Kawazoe, Phys. Rev. B **66**, 064412 (2002).
[10] H. B. Wu, S. R. Desai, and L. S. Wang, Phys. Rev. Lett. **76**, 212 (1996).
[11] S. R. Liu, H. J. Zhai, M. Castro, and L. S. Wang, J. Chem. Phys. **118**, 2108 (2003).
[12] S. R. Liu, H. J. Zhai, and L. S. Wang, Phys. Rev. B **64**, 153402 (2001).
[13] S. R. Liu, H. J. Zhai, and L. S. Wang, Phys. Rev. B **65**, 113401 (2002).
[14] S. R. Liu, H. J. Zhai, and L. S. Wang, J. Chem. Phys. **117**, 9758 (2002).
[15] L. S. Wang, X. Li, and H. F. Zhang, Chem. Phys. **262**, 53 (2000).
[16] L. Lian, C.-X. Su, and P. B. Armentrout, J. Chem. Phys. **97**, 4084 (1992).
[17] M. Castro, S. R. Liu, H. J. Zhai, and L. S. Wang, J. Chem. Phys. **118**, 2116 (2003).
[18] S. Y. Wang, W. H. Duan, D. L. Zhao, and C. Y. Wang, Phys. Rev. B **65**, 165424 (2002).
[19] O. Jepson, Phys. Rev. B **12**, 2988 (1975).
[20] P. C. Hohenberg and W. Kohn, Phys. Rev. **136**, B864 (1964).
[21] W. Kohn and L. J. Sham, Phys. Rev. **140**, A1133 (1965).
[22] B. Delley, J. Chem. Phys. **92**, 508 (1990).
[23] B. Delley, J. Chem. Phys. **94**, 7245 (1991).
[24] S. H. Wei, Z. Zeng, J. Q. You, X. H. Yan, and X. G. Gong, J. Chem. Phys. **113**, 11127 (2000).
[25] J. P. Perdew and Y. Wang, Phys. Rev. B **45**, 13244 (1992).
[26] A. D. Becke, Phys. Rev. A **38**, 3098 (1988).
[27] V. L. Moruzzi, J. F. Janak, and A. R. Williams, *Calculated Electronic Properties of Metals* (Pergamon, New York, 1978).

Energetics and local spin magnetic moment of single 3,4*d* impurities encapsulated in an icosahedral Au_{12} cage

Shan-Ying Wang,[1,2,*] Jing-Zhi Yu,[1] Hiroshi Mizuseki,[1] Qiang Sun,[3] Chong-Yu Wang,[2] and Yoshiyuki Kawazoe[1]
[1]*Institute for Materials Research, Tohoku University, Aoba-ku, Sendai 980-8577, Japan*
[2]*Department of Physics, Tsinghua University, Beijing 100084, People's Republic of China*
[3]*Physics Department, Virginia Commonwealth University, Richmond, Virginia 23284-2000, USA*
(Received 7 April 2004; revised manuscript received 1 June 2004; published 21 October 2004)

The energetics and local spin magnetic moment of a single 3,4*d* impurity (Sc-Ni, Y-Pd) encapsulated in an icosahedral Au_{12} cage have been studied theoretically by using a real-space first-principles cluster method with generalized gradient approximation for exchange-correlation functional. The relativistic effect is considered by scalar relativistic pseudopotentials. All doped clusters show unexpected large relative binding energies compared with icosahedral Au_{13} cluster. The smallest and the largest values appear at Pd and Zr, 2.186 and 7.791 eV per cluster, respectively, indicating doping could stabilize the icosahedral Au_{12} cage and promote the formation of a new binary alloy cluster. Comparatively large magnetic moments are observed for 3*d* elements Cr, Mn, Fe, Co, and Ni (2.265, 3.512, 3.064, 1.947, and 0.943 μ_B), and 4*d* elements Tc, Ru, and Rh (0.758, 1.137, and 0.893 μ_B). The density of states and the relativistic effects on electronic structure are discussed.

DOI: 10.1103/PhysRevB.70.165413 PACS number(s): 31.15.Ar, 36.40.Cg, 36.40.Qv

I. INTRODUCTION

Single transition metal element isolated in an *sp* metal host is a classical ideal system for studying how the *d* electron interact with nearly free electron gas to form a local magnetic moment (LMM).[1–4] The recent advanced synthesis techniques are making scientists able to explore such a problem in many different types of system. For example, it has been shown experimentally that transition metal element can also display unusual large LMM when absorbed on or embedded into an *sp* metal surface.[5,6] The LMM of transition metal element is rather sensitive to the environment, and adjusted dramatically by the shape and size of the environment formed by the host atoms. From this point of view, one can design many different types of system for studying the local magnetism problem. For example, a single 3,4*d* impurity encapsulated in an *sp* metal cage may be an interesting system. The idea of doping an impurity into a cluster cage initially appeared in the work[7,8] of Callaway and Dunlap, and then extended explicitly by Gong, Kumar, Sun, and Kawazoe as studying the stability and local magnetic properties of 3,4*d* impurities encapsulated in icosahedral Al_{12}, Cu_{12}, and Ag_{12} cages.[9–11] These theoretical works predicted that some 3,4*d* impurities could show relatively large local spin magnetic moments (LSMM's) when encapsulated in an *sp* metal cage.

On the other hand, the studies on pure noble metal element and its binary alloy clusters have attracted considerable interest in recent years. A more recent experiment[12] did prove the presence of small binary alloy Au_NX clusters (X =Sc, Ti, V, Cr, Mn, Fe, Co, and Ni). In contrast to pure Cu and Ag clusters, small pure Au cluster is believed[13,14] to favor three-dimensional amorphous or planar configurations. While from technical viewpoint, high-symmetrical clusters sometimes are necessary as building blocks in nanostructures such as nanograin-film and nanocrystalline materials. For the unstable icosahedral Au_{12} cage (Au_{13}), doping an 3,4*d* impurity (substituting the center Au atom with an 3,4*d* impurity) may be a good way to stabilize the structure. This has been proved feasible for Mo by a recent experiment.[15]

The above research background motivates the present study. As a continuation of previous theoretical research work, we have investigated the energetics and LSMM of a single 3,4*d* impurity encapsulated in an icosahedral Au_{12} cage by employing a state-of-the-art first-principles method called density functional for molecules (DMol)[16,17] based on density functional theory (DFT).[18,19] The case of the impurity atom substituting a surface Au atom is not included in the present study. It will be seen that some 3,4*d* impurities do display very large LSMM in the icosahedral Au_{12} cage. The calculated binding energy suggests that doping an 3,4*d* element will be a feasible way to stabilize icosahedral Au_{12} cage to yield a binary alloy cluster. The LSMM and electronic structure are discussed in detail within the spin DFT scheme. As having been frequently found in many other kinds of low-dimensional systems such as surface, overlayer, sandwich, superlattice and adatom absorbed on a surface, we believe that large magnetic moment could also be found in a binary alloy cluster.

II. METHOD AND COMPUTATIONAL DETAIL

DMol is a widely used real-space first-principles cluster method, and has been successfully applied to many problems such as structural stability of molecular clusters, chemisorption and surface reconstruction. It can perform accurate and efficient self-consistent calculation and structural optimization. The equilibrium structure can be obtained by relaxing atom until the energy gradients are deemed to be zero.

To ensure the results accurate and reliable, we have chosen an exchange correlation functional proposed by Perdew (PW91),[20] a general gradient approximation (GGA) that has been successfully applied to the studies on transition metal systems, for instance, medium-size Mn clusters.[21] The rela-

TABLE I. The binding energies (BE, in eV) and equilibrium distances (r, in Å) of 3,4d and Au dimers obtained by using a basis set composed of double numerical basis with polarized functions.

	Theory		Experiment[a]	
	BE	r	BE	r
Ti_2	4.250	1.968	1.54±0.19	1.942
V_2	5.355	1.799	2.75	1.783
Cr_2	0.638	1.648	1.53±0.06	1.679
Mn_2	0.802	2.580	0.3±0.3	3.4
Fe_2	3.392	1.994	1.15±0.09	2.02
Ni_2	5.535	2.107	2.04	2.155
Nb_2	4.458	2.137	5.22±0.31	2.078
Mo_2	2.617	1.990	4.474±0.010	1.94
Rh_2	5.619	2.260	2.460±0.005	2.28
Au_2	2.165	2.489	2.29	2.472

[a]The experimental data can be found in Refs. 32–44.

tivistic effect is significant for Au. Currently, DMol can consider scalar relativistic effects, such as Darwin and mass velocity, by either effective core potential calculation or all-electron calculation. The properties of those heavier atoms are reproduced using an essentially nonrelativistic Hamiltonian including pseudopotentials representing scalar relativistic effects.[22–24] A basis set composed of double numerical basis (3d,4s doubled for 3d impurity and 4d,5s doubled for 4d impurity, and 5d,6s doubled for Au) with polarized functions (4p for 3d impurity and 5p for 4d impurity, and 6p for Au) is adopted, and all-electron spin-unrestricted calculations are performed. These can ensure much better descriptions on binding energy and magnetism, and minimize the influence of basis on calculation results to the least. The quality of the basis set was discussed in detail in the previous literatures.[16,17] We have further checked the basis set by calculations on some 3,4d and Au dimers. It can be seen from Table I that the present selected basis set can give reasonable results except for Mn dimer, comparable to the various different basis sets used in the recent *ab initio* studies.[25,26] Note all these theoretical studies failed in Mn dimer and have some errors on binding energy.

Figure 1 shows the geometrical structure of a single 3,4d impurity encapsulated in an icosahedral Au_{12} cage. In structural optimization, the 12 Au atoms are relaxed freely under I_h symmetry. The energy gradient and atomic displacement are converged to 3×10^{-3} eV Å^{-1} and 1×10^{-4} Å respectively. For self-consistent field iteration, the charge density is converged to 1×10^{-5}, which corresponds to a total energy convergence of 1×10^{-6} eV. The order of the multipolar function used for fitting charge density and solving Coulomb potential is set to be one greater than the maximum angular momentum in the basis set. About 1500 fixed integration points around each atom are used. The binding energy (BE) is defined as

$$\mathrm{BE} = E_a - E_t,$$

where E_a is the sum of the total energies of all single atoms and E_t is the total energy of the cluster.

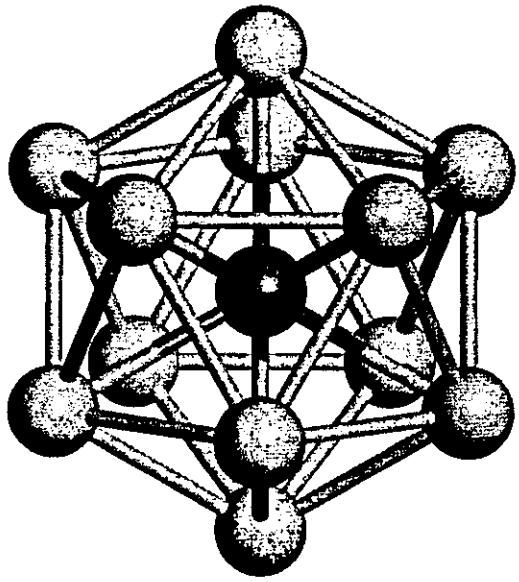

FIG. 1. The cluster model of a single 3,4d impurity encapsulated in an icosahedral Au_{12} cage. The center dark ball represents the 3,4d impurity and the outside 12 gray balls represent Au atoms.

III. RESULTS AND DISCUSSIONS

The calculated results are summarized in Table II with that on icosahedral Au_{13} for comparison. It is interesting to know if the doped icosahedral Au_{12} could be stabilized at a three-dimensional shape. This can be simply concluded by comparing the BE of doped Au_{12} with that of pure Au_{13}. As well known, energy difference between two isomers is rather significant if the value exceeds 1 eV per cluster. From Table II we can see that the BE's of the doped Au_{12} clusters are surprisingly larger than that of pure icosahedral Au_{13}. The smallest and the largest relative BE's compared with pure icosahedral Au_{13} appear at Pd and Zr, 2.186 and 7.791 eV per cluster, respectively. Clusters doped with Ti, V, and Ni also show very large relative BE's beyond 7.0 eV per cluster. The relative BE's of the rest doped clusters are beyond 3.2 eV per cluster. Even though it is not much strict to make conclusions only from BE, these unusual large relative BE's still convince us that doping a single 3,4d impurity could make the icosahedral Au_{12} cage stable, and form a new binary alloy cluster of three-dimensional rather than planar structure.

Local magnetism is another interesting problem in these doped systems. For 3d impurities Sc, Ti, and V just show small LSMM's while relatively large LSMM's are observed from Cr to Ni. Mn has the largest one, about 3.51 μ_B and then Fe about 3.06 μ_B. These features basically extend to 4d impurities except that all their LSMM's decrease to a certain extent and an "abnormal" case occurs to Mo. The former part of elements Y, Zr, and Nb still show small LSMM's and the latter ones from Tc to Pd show relatively strong LSMM's. Ru has the largest LSMM about 1.14 μ_B and Rh is next to it, about 0.89 μ_B. It is meaningful to know why these 3,4d impurities display so different LSMM's as being encapsulated in an icosahedral Au_{12} cage. We can give a simple qualitative explanation by considering the chemical bonding

TABLE II. The calculated data on a single 3,4*d* impurity encapsulated in an icosahedral Au_{12} cage: the cluster binding energy (BE, in eV), the cluster radius R (in Å), the HOMO and LUMO states (symmetry and spin), the HOMO-LUMO gap ΔE (in eV), the electron occupation number n in the HOMO, the total magnetic moment M_t of cluster (in μ_B), and the atomic magnetic moment M (in μ_B). Symbol + and − denote spin-up and spin-down states, respectively. Data on pure icosahedral Au_{13} and the relative binding energy (RBE, in eV) compared to Au_{13} are included. Some data obtained by nonrelativistic all-electron calculations are given in the parentheses for comparison.

	BE	RBE	R	HOMO	LUMO	ΔE	n	M_t	$M_{3,4d}$	M_{Au}
Sc	33.796(14.342)	5.965(4.682)	2.690(2.975)	HG(−)	AG(+)	1.973(1.315)	2	3	0.190(0.765)	0.234
Ti	35.320(15.374)	7.489(5.714)	2.659(2.943)	HG(−)	HG(+)	1.814(1.320)	3	2	0.265(1.286)	0.145
V	34.901(15.409)	7.070(5.749)	2.643(2.928)	HG(−)	HG(+)	1.241(0.982)	4	1	0.480(2.547)	0.043
Cr	31.507(12.631)	3.676(2.971)	2.642(2.925)	HG(−)	HG(+)	0.790(0.818)	5	0	2.265(3.646)	−0.189
Mn	31.061(12.526)	3.230(2.866)	2.648(2.920)	HG(+)	HG(−)	1.300(0.508)	1	1	3.512(3.785)	−0.209
Fe	32.035(13.585)	4.204(3.925)	2.643(2.908)	HG(+)	HG(−)	0.758(0.540)	2	2	3.064(2.826)	−0.089
Co	32.239(14.163)	4.408(4.503)	2.637(2.900)	HG(+)	HG(−)	0.469(0.414)	3	3	1.947(1.608)	0.088
Ni	32.009(14.321)	4.178(4.661)	2.638(2.900)	HG(+)	HG(−)	0.362(0.365)	4	4	0.943(0.665)	0.255
Y	32.934(14.366)	5.103(4.706)	2.760(3.039)	HG(−)	T2U(+)	2.116(1.579)	2	3	0.144(0.815)	0.238
Zr	35.622(16.334)	7.791(6.674)	2.722(2.996)	HG(−)	AG(+)	2.077(1.625)	3	2	0.163(0.887)	0.153
Nb	35.125(15.511)	7.294(5.851)	2.693(2.967)	HG(−)	HG(+)	2.016(1.715)	4	1	0.135(0.818)	0.072
Mo	32.675(14.442)	4.844(4.782)	2.677(2.945)	HG(±)	HG(±)	1.578(1.705)	10	0	0.000(0.000)	0.000
Tc	32.892(15.423)	5.061(5.763)	2.676(2.939)	HG(+)	HG(−)	0.242(0.233)	1	1	0.758(1.000)	0.020
Ru	31.184(14.720)	3.353(5.060)	2.678(2.938)	HG(+)	HG(−)	0.347(0.262)	2	2	1.137(0.961)	0.072
Rh	31.314(14.463)	3.483(4.803)	2.681(2.938)	HG(+)	HG(−)	0.323(0.274)	3	3	0.893(0.581)	0.176
Pd	30.017(11.790)	2.186(2.130)	2.688(2.950)	HG(+)	HG(−)	0.309(0.329)	4	4	0.460(0.233)	0.295
Au	27.831(9.660)		2.700(2.996)	HG(+)	HG(−)	0.358(0.408)	5	5	0.223(0.034)	0.398

and the magnetic interaction, two important opposite and competitive factors for BE of transition metal cluster or cluster including transition metal elements. A cluster usually tends to enhance its BE and to make the structure stable and compact by forming chemical bonds as more as possible. This, however, is not the most efficient way even the chemical bonding making the most contributions to BE. The magnetic interaction sometimes also plays an important role. To increase the exchange-splittings of *d* orbitals by reducing the strength of some chemical bonds can further enhance the BE. As a result of the competition between the two factors, a cluster finally reaches its stable structural and magnetic states. The former part of 3*d* elements such as Sc, Ti, and V show weak LSMM's because of the activities of their *s*,*p* electrons, which result in strong hybridizations that can suppress the occurrence of large exchange splittings of 3*d* orbitals, reducing the magnetic interaction. For the latter part of 3*d* elements from Cr to Ni, the magnetic interaction becomes strong enough to yield comparatively large LSMM. We can see that Cr, Mn, and Fe even make the polarization of Au_{12} cage antiparallel with their LSMM's. The relative weakness of LSMM's of 4*d* impurities is mainly related to their large atomic radii. Large overlaps between the atomic orbitals could not promote the formation of LSMM. The case of Mo seems "abnormal." The magnetic interaction is completely suppressed by the chemical bonding and all electrons are paired to give a closed-shell system. Our results on Mo are consistent with the experiment.[15] It is worthwhile to mention another similar theoretical study on an 5*d* element of same column W,[27] where a highly stable closed-shell structure of W encapsulated in an icosahedral Au_{12} cage is predicted.

Compared with the doped clusters, Au_{13} has the highest total magnetic moment. The individual Au atom in it, however, just shows small magnetic moment. The most number of unpaired electrons rather than the largest exchange-splittings result in the highest total magnetic moment of Au_{13}. Certainly a small exchange-splitting of molecular orbital is necessary in this regard. This is physically reasonable since Au is not a magnetic element. The number of paired electrons in the HOMO and its neighboring occupied molecular orbitals increases from Sc to Cr and Y to Mo, and decreases from Mn to Ni and Tc to Pd. Consequently, the total magnetic moment of cluster decreases from Sc to Cr and Y to Mo, but increases from Mn to Ni and Tc to Pd. This looks similar to the occupation feature of the "rigid band" in a alloy with different impurities. Nevertheless, we should notice that the LSMM for each individual atom in these doped clusters is not proportional to the total magnetic moment of cluster. Such case is easily seen in the spin antiparallel systems such as Cr, Mn, and Fe doped clusters. For case of Cr, the total magnetic moment of cluster is zero. The Cr impurity, however, has a rather large LSMM (2.265 μ_B).

The size effect on LSMM is always dramatic. To see this, here we draw a comparison between the LSMM in the cluster and that in the solid for all 3*d* impurities except for Sc. Compared with the nearest neighboring interatomic distances in the solid (about 2.89, 2.62, 2.50, 2.48, 2.50, and 2.49 Å for hcp Ti, bcc V, bcc Cr, bcc Fe, hcp Co, and fcc Ni, respectively), the interatomic distance between the 3*d* impurity and Au (the cluster radius shown in Table II) decreases by about 8% for Ti, but increases by about 5% for Cr, Fe, Co, and Ni, and changes slightly for V. The bulk hcp Ti and bcc V are

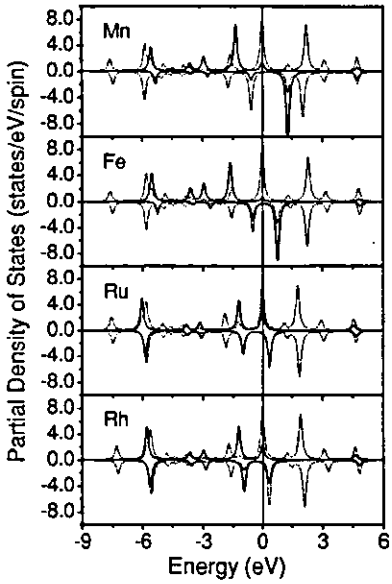

FIG. 2. The spin-dependent partial density of states for Mn, Fe, Ru, and Rh encapsulated in an icosahedral Au_{12} cage. The spin-up and the spin-down states are displayed in the up panel (plus value) and down panel (minus value), respectively. The solid line represents the *d* states of transition metal element, and the dashed line represents the *s* states of Au. Fermi level is shifted to zero.

Pauli paramagnets and hardly show any LSMM.[28] While in cluster they can have small LSMM)s, about 0.27 and 0.48 μ_B, respectively. The bcc Cr is thought to be a spin density wave system with just a small amplitude of LSMM (the maximum is about 0.60 μ_B).[28] Mn, Fe, Co, and Ni are strong magnetic elements. They can show net LSMM's at complex cubic (the maximum is about 1.90 μ_B), bcc (2.13 μ_B), hcp (1.52 μ_B), and fcc (0.57 μ_B) structures, respectively.[28,29] From Cr to Ni, obviously all their LSMM's are enhanced greatly when they are encapsulated in an icosahedral Au_{12} cage, where the increased interatomic distance plays an important role.

For system made up of transition and noble metal elements, orbital usually makes little contributions to the magnetic moment. A spin exchange-splitting picture based on spin DFT is enough to give a good description on such problem. As an illustration, we present in Fig. 2 the spin-dependent partial density of states (PDOS) for four typical transition metal elements Mn, Fe, Ru, and Rh. The PDOS is calculated by broadening the energy levels ε_i^σ of molecular orbitals (σ denote spin state) by using a line-shape function Lorentzian with width δ=0.1 eV as follows:

$$\mathrm{DOS}_{anl}^{\sigma}(E) = \sum_i P_{i,anl}^{\sigma} \frac{\delta/\pi}{(E-\varepsilon_i^{\sigma})^2 + \delta^2},$$

where $P_{i,anl}^{\sigma}$ (α denotes atom, *n* and *l* are, respectively, main and angular quantum numbers) is the state component of atomic orbital in molecular orbital (ε_i^{σ}) obtained by Mulliken analysis.[30] Obviously, strong hybridizations between the *d* orbitals of 3,4*d* impurity and the 6*s* orbital of Au occur in a wide energy range, from about −5.5 to 5.0 eV. A strong resonant peak appearing at a rather low energy site −5.5 eV

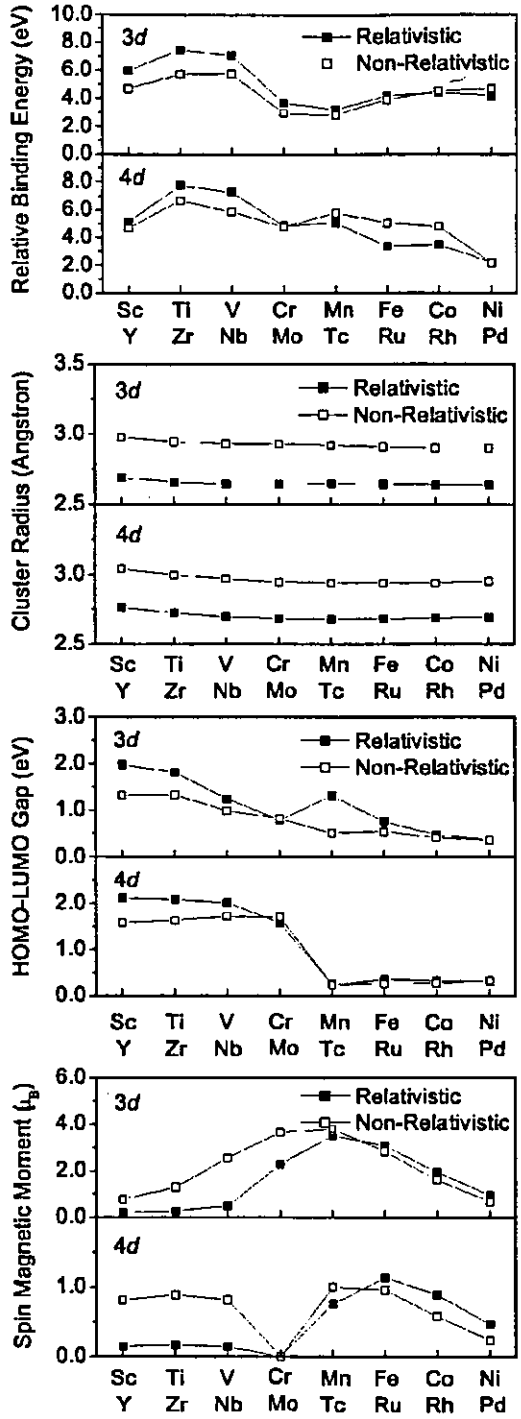

FIG. 3. The relativistic effects on the relative binding energy (compared with icosahedral Au_{13}), the cluster radius, the HOMO-LUMO gap, and the spin magnetic moment.

seems unusual since the *d* states are usually localized around the Fermi level. The *d* orbitals of Mn and Fe show larger exchange splittings than those of Ru and Rh near the Fermi level, resulting in larger magnetic moments. The *s-d* hybridizations and exchange-splittings of *d* orbitals are the main features of interaction in these doped clusters.

Relativistic effects (RE's) are particularly important for Au_{13}.[31] Table II and Fig. 3 present, respectively, the results

obtained by relativistic and non-relativistic all-electron calculations and their comparisons. The RE's corrections on the results are not so systematic but obvious. They are more significant for the former part than for the latter part of $3,4d$ impurities. The RE's correction on relative BE (compared with icosahedral Au_{13}) is remarkable for all $3,4d$ impurities except for Co, Mo, and Pd. It yields the enhanced relative BE's for the former part of $3,4d$ impurities from Sc to Cr and Y to Nb, but the weakened relative BE's for the latter part of $4d$ impurities from Tc to Rh. The bond length is rather sensitive to the RE's correction for all the doped clusters, whose structures become more compact if the RE's correction is considered. The RE's corrections on these cluster radii are close to a stable value, about 0.27 Å. The change of HOMO-LUMO gap is significant for impurities from Sc to V and Y to Nb, and also for Mn and Fe. The RE's correction gives enhanced HOMO-LUMO gaps of these impurities. The LSMM is also sensitive to RE's correction for the former part of $3,4d$ impurities from Sc to Cr and Y to Nb, whose LSMM's are weakened greatly. The LSMM's of impurities from Fe to Ni and Ru to Pd, however, are enhanced to some extent. The results for Mo seem insensitive to the RE's correction except for cluster radius.

IV. SUMMARY

Cluster method based on DFT is used to explore the energetics and local spin magnetic moment of a single $3,4d$ impurity encapsulated in an icosahedral Au_{12} cage. All doped clusters show unexpected large relative binding energies compared with icosahedral Au_{13} cluster, indicating a high possibility of forming a new binary alloy cluster. Large spin magnetic moments are observed for $3d$ impurities Cr, Mn, Fe, Co, and Ni, and $4d$ impurities Tc, Ru, and Rh due to large exchange splittings of d orbitals. Strong hybridizations between the d orbitals of $3,4d$ impurity and the $6s$ orbital of Au occur. The correction of relativistic effect is very important for electronic structure.

ACKNOWLEDGMENTS

The authors would like to express their sincere thanks to the crew of Center for Computational Materials Science of the Institute for Materials Research, Tohoku University for their continuous support of the supercomputing facilities.

*Electronic address: sywang@imr.edu

[1] D. van der Marel, C. Westra, and G. A. Sawatzky, Phys. Rev. B **31**, 1936 (1985).
[2] D. Riegel, L. Büermann, K. D. Gross, M. Luszik-Bhadra, and S. N. Mishra, Phys. Rev. Lett. **61**, 2129 (1988).
[3] N. Papanikolaou, N. Stefanou, R. Zeller, and P. H. Dederichs, Phys. Rev. B **46**, 10858 (1992).
[4] R. N. Nogueira and H. M. Petrilli, Phys. Rev. B **63**, 012405 (2000).
[5] H. Beckmann and G. Bergmann Phys. Rev. Lett. **83**, 2417 (1999).
[6] P. Gambardella, S. S. Dhesi, S. Gardonio, C. Grazioli, P. Ohresser, and C. Carbone, Phys. Rev. Lett. **88**, 047202 (2002).
[7] D. Bagayoko, N. Brener, D. Kanhere, and J. Callaway, Phys. Rev. B **36**, 9263 (1987).
[8] B. I. Dunlap, Z. Phys. D: At., Mol. Clusters **19**, 255 (1991).
[9] X. G. Gong and Vijay Kumar, Phys. Rev. B **50**, 17701 (1994).
[10] Q. Sun, X. G. Gong, Q. Q. Zheng, D. Y. Sun, and G. H. Wang, Phys. Rev. B **54**, 10896 (1996).
[11] Q. Sun, Q. Wang, J. Z. Yu, Z. Q. Li, J. T. Wang, and Y. Kawazoe, J. Phys. I **7** 1233 (1997).
[12] S. Neukermans, E. Janssens, H. Tanaka, R. E. Silverans, and P. Lievens, Phys. Rev. Lett. **90**, 033401 (2003).
[13] J. Oviedo and R. E. Palmer, J. Chem. Phys. **117**, 9548 (2002).
[14] Han Myoung Lee, Maofa Ge, B. R. Sahu, P. Tarakeshwar, and Kwang S. Kim, J. Phys. Chem. B **107**, 9994 (2003).
[15] Xi Li, Boggavarapu Kiran, Jun Li, Hua-Jin Zhai, and Lai-Sheng Wang, Angew. Chem., Int. Ed. **41**, 4786 (2002).
[16] B. Delley, J. Chem. Phys. **92**, 508 (1990).
[17] B. Delley, J. Chem. Phys. **94**, 7245 (1991).
[18] P. C. Hohenberg and W. Kohn, Phys. Rev. **136**, B864 (1964).
[19] W. Kohn and L. J. Sham, Phys. Rev. **140**, A1133 (1965).
[20] J. P. Perdew and Y. Wang, Phys. Rev. B **45**, 13244 (1992).
[21] Tina M. Briere, Marcel H. F. Sluiter, V. Kumar, and Y. Kawazoe, Phys. Rev. B **66**, 064412 (2002).
[22] B. Delley, Int. J. Quantum Chem. **69**, 423 (1998).
[23] L. F. Pacios and P. A. Christiansen, J. Chem. Phys. **82**, 2664 (1985).
[24] M. M. Hurley, L. F. Pacios, P. A. Christiansen, R. B. Ross, and W. C. Ermler, J. Chem. Phys. **84**, 6840 (1986).
[25] S. Yanagisawa, T. Tsuneda, and K. Hirao, J. Chem. Phys. **112**, 545 (2000).
[26] S. Yanagisawa, T. Tsuneda, and K. Hirao, J. Comput. Chem. **22**, 1995 (2001).
[27] Pekka Pyykkö and Nino Runeberg, Angew. Chem., Int. Ed. **41**, 2174 (2002)
[28] *Landolt-Bornstein, Numerical Data and Functional Relationships in Science and Technology*, New Series, edited by K.-H. Hellwege, and O. Madelung, *Group III: Crystal and Solid State Physics*, Vol. 19, Subvol. a (Springer-Verlag, Heidelberg, 1986).
[29] *Landolt-Bornstein, Numerical Data and Functional Relationships in Science and Technology*, New Series, Group III, Vol. 32, Supplement to Vol. 19, Subvol. A, edited by H. P. J. Wijn (Springer-Verlag, Heidelberg, 1997).
[30] R. S. Mulliken, J. Chem. Phys. **23**, 1833 (1955).
[31] P. Pyykkö, Chem. Rev. (Washington, D.C.) **88**, 563 (1988).
[32] H. Åkeby and L. G. M. Pettersson, J. Mol. Spectrosc. **159**, 17 (1993).
[33] L. M. Russon, S. A. Heidecke, M. K. Birke, J. Conceicao, M. D. Morse, and P. B. Armentrout, J. Chem. Phys. **100**, 4747 (1994).
[34] E. M. Spain, J. M. Behm, and M. D. Morse, J. Chem. Phys. **96**, 2511 (1992).
[35] B. Simard, M.-A. Lebeault-Dorget, A. Marijnissen, and J. J. ter Meulen, J. Chem. Phys. **108**, 9668 (1998).
[36] S. K. Loh, L. Lian, D. A. Hales, and P. B. Armentrout, J. Phys.

Chem. **92**, 4009 (1988).
[37] J. C. Pinegar, J. D. Langenberg, C. A. Arrington, E. M. Spain, and M. D. Morse, J. Chem. Phys. **102**, 666 (1995).
[38] E. A. Rohlfing and J. J. Valentini, J. Chem. Phys. **84**, 6560 (1986).
[39] K. P. Huber and G. Herzberg, *Constants of Diatomic Molecules* (Van Nostrand Reinhold, New York, 1979), Vol. 4.
[40] A. M. James, P. Kowalczyk, R. Fournier, and B. Simard, J. Chem. Phys. **99**, 8504 (1993).
[41] D. A. Hales, L. Lian, and P. B. Armentrout, Int. J. Mass Spectrom. Ion Processes **102**, 269 (1990).
[42] S. Lee, D. M. Bylander, and L. Kleinman, Phys. Rev. B **37**, 10035 (1988),
[43] M. D. Morse, Chem. Rev. (Washington, D.C.) **86**, 1049 (1986).
[44] J. D. Langenberg and M. D. Morse, J. Chem. Phys. **108**, 2331 (1998).

Transactions of the Materials Research Society of Japan VOL.29 15-18 (2004)

All-electron calculations on MgO cluster (n=1-10) with Tohoku University Mixed-Basis Program TOMBO

Amit Jain*, Vijay Kumar*,** and Yoshiyuki Kawazoe*
* Institute for Materials Research, Tohoku University, 2-1-1 Katahira, Aoba-ku, Sendai 980-8577, Japan
Fax: 81-22-215-2052, e-mail: amitjain@imr.edu
** Dr. Vijay Kumar Foundation, 45 Bazaar Street, K. K. Nagar (West), Chennai 600 078, India

All-electron mixed-basis approach which uses both plane wave and atomic orbitals as the basis functions, has been used to do *ab initio* study of $(MgO)_n$ cluster n=1-10. For this purpose Tohoku Mixed-Basis Program TOMBO based on the local density approximation (LDA) is used to optimize the structures of MgO clusters. Calculated electronic structures and bond length are in good agreement with available experiment data. TOMBO program, when used in parallel environment, makes the structure optimization calculation quite fast with increase in MgO cluster size.

Key words: MgO Clusters, all-electron mixed-basis method, structure optimization, parallel processing

1. INTRODUCTION

Currently there is much focus on materials research at the nanoscale because of the important role these are expected to play in future technologies. It is important to develop a fundamental understanding of the growth behavior of matter in going from atoms to bulk. As the structures and bonding at the nanoscale are generally different from bulk, studies of clusters provide an interesting way to understand the evolution of the properties of materials from atoms to the bulk condensed state. Therefore, this has prompted numerous studies of cluster properties as a function of size.

Recently there has been an intense interest in the study of metal oxide clusters. Often clusters of such compounds are considered to be bulk fragments. However, their structure and properties could be different at the nanoscale. Here we consider clusters of magnesium oxide. There have been very few *ab initio* studies on small MgO clusters[1][4]. Also empirical methods have been used considering primarily ionic bonding[5]. However, the understanding of the growth behavior is still not well understood. A survey of the previous studies gave a very contradictory view of the MgO cluster structures and bonding behavior. In this light we studied MgO clusters using all electron mixed basis approach. As one expects significant charge transfer from Mg atoms to O, it is considered appropriate to include the inner orbitals that are best represented in an all electron calculation. For this, we have used Tohoku University Mixed-Basis program TOMBO for optimizing the MgO cluster structures.

2. ALL-ELECTRON MIXED-BASIS METHOD TOMBO

The mixed-basis means that the combination of both plane waves (PWs) and atomic orbitals (AOs) is used as basis function. The introduction of AOs considerably reduces the load of the PW expansion method[7],[8]. In the mixed-basis method, the electronic wavefunctions are expanded using both PWs and AOs, making an accurate description of both local and extended electronic states, where not only valance AOs but also core AOs are incorporated to describe all-electrons without using pseudopotentials.

In present study, structure optimization of MgO clusters has been done using TOMBO, which is a program based on all-electron mixed basis method developed at Tohoku University. TOMBO uses optimal linear and Broyden mixing of the electronic charge density and can be used to do structural optimization and molecular dynamic simulations, vibrational analysis, including IR activity, Born effective charges and can simulate Fermi contact interaction and dipole moment. In TOMBO the Coulomb and exchange-correlation potentials are evaluated separately for PW and for AO, respectively, in reciprocal space and in real space. So PW-PW, AO-PW and AO-AO contributions to the charge density and the potential are calculated separately [9]. We have used local density approximation (LDA) for this study.

To take advantage of the multiprocessor architectures of most modern supercomputers, TOMBO code has been SIMD-parallelized by means of message passing interface (MPI) calls in the most computationally demanding subroutines e.g. for computing the product of the Hamiltonian and the wavefunction, for computing FFTs, for orthogonalizing the Hamiltonian, and for transforming the representation of the wavefunction on orthogonal and non-orthogonal bases[9]. TOMBO program is capable of very large scale calculations when used in parallel computing environment[10].

3. RESULTS AND DISCUSSION

3.1 Structures

We calculated the optimized clusters of MgO with LDA. The unit cell is chosen as a cube of 1.6 nm width. We have used Hitachi SR8000/64 512 parallel 1 teraflop supercomputer to do these all-electron mixed basis calculations.

The results of the structures of different isomers studied here, as well as bond length, total energy and energy per molecule are given in Fig. 1, Fig. 2, Table I

and Table II. The red balls represent Oxygen and green balls represent Magnesium in Fig. 1 and Fig. 2.

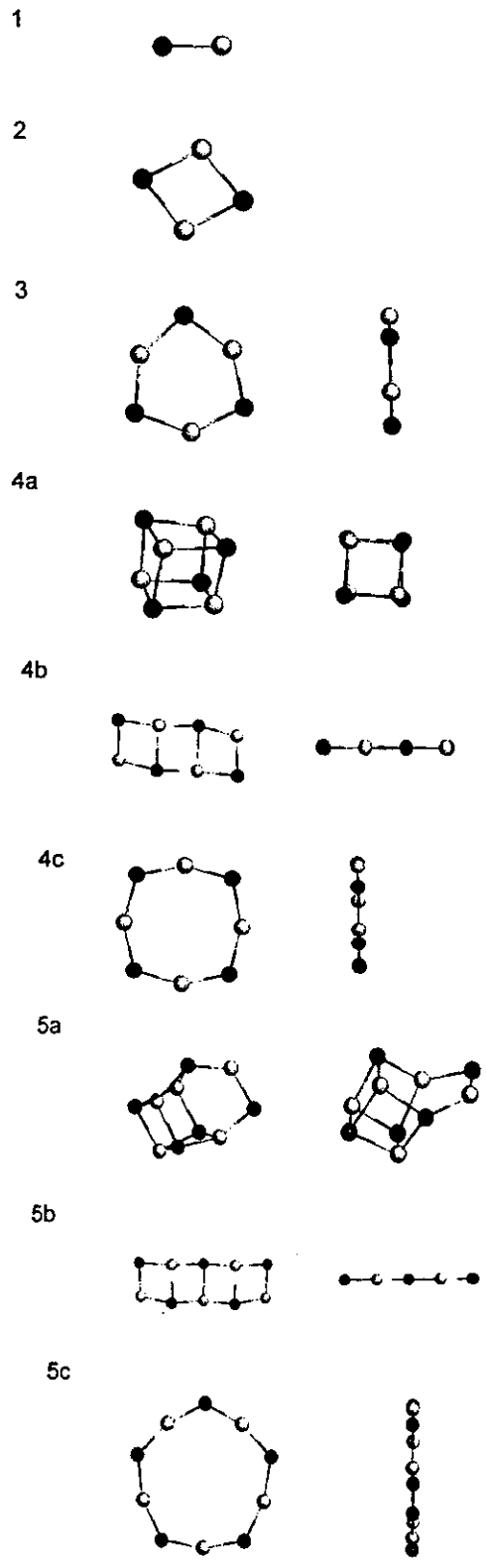

Fig. 1 Optimized structures of MgO n=1-5. From n=3-5 front view is shown in the left side and side view of the structures is shown in right side

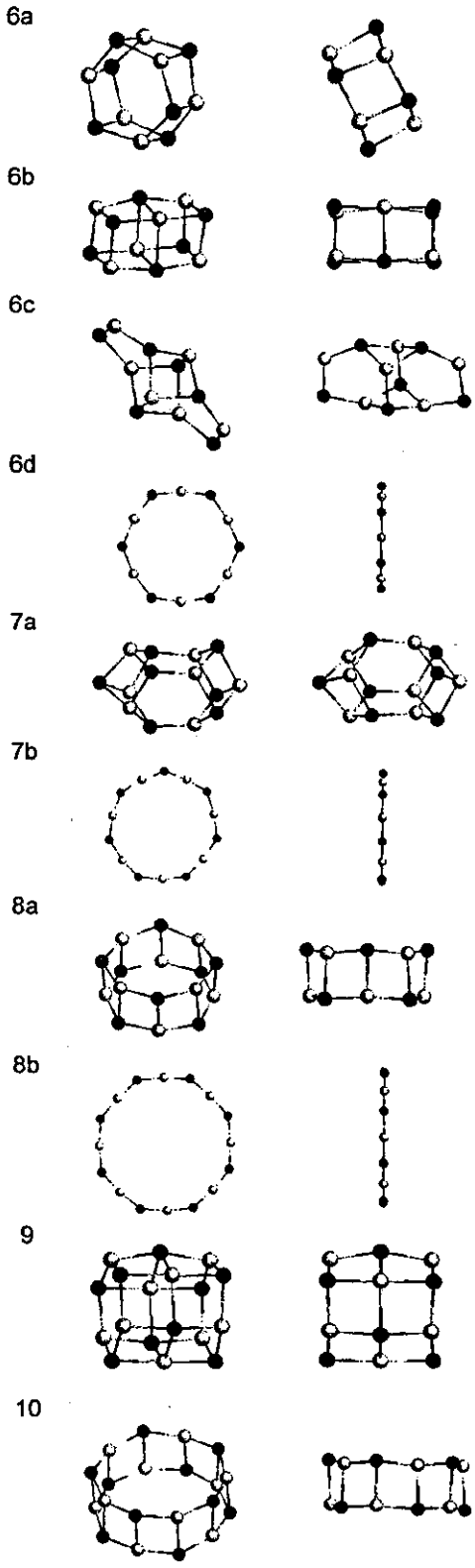

Fig. 2 Optimized structures of MgO n=6-10. Front/top view is shown in the left side and side view of the structures is shown in right side

Table I Structure and Bond length (Å) of MgO clusters

n	structure	Bond length (Å)
1	monomer	1.75
2	2*2*1	1.88
3	ring	1.83
4a	2*2*2	1.95
4b	4*2*1	1.84, 2.08, 1.91, 1.85, 1.89
4c	ring	1.82
5a	distorted cube open at one side	1.94, 1.93, 1.95, 1.97, 1.98, 1.86, 1.80, 1.89
5b	5*2*1	1.84, 2.09, 1.99, 1.85, 1.91, 1.89
5c	ring	1.815
6a	ring*2	1.91, 1.99
6b	3*2*2	1.94, 2.11, 1.91, 1.97
6c	distorted cube open at two sides	1.81, 1.90, 1.86, 1.89, 1.96, 1.98
6d	ring	1.81
7a	cage	1.93, 1.94, 1.87
7b	ring	1.80
8a	ring*2	1.89, 2.00
8b	ring	1.80
9	ring*3	1.90, 2.05
10	ring*2	1.89, 2.00

Table II Total energy (eV) and Energy per MgO molecule (eV) for MgO clusters n=1-10

n	Total Energy	Energy/molecule
1	7440.07	7440.07
2	14896.74	7448.37
3	22348.29	7449.43
4a	29800.68	7450.17
4b	29799.41	7449.85
4c	29799.00	7449.75
5a	37251.22	7450.24
5b	37250.80	7450.16
5c	37249.33	7449.87
6a	44704.70	7450.78
6b	44704.58	7450.76
6c	44701.85	7450.31
6d	44699.53	7449.92
7a	52156.30	7450.90
7b	52149.66	7449.95
8a	59607.71	7450.96
8b	59600.12	7450.02
9	67061.00	7451.22
10	74510.29	7451.03

When these results are compared with the experimental results, calculated bond length of the MgO monomer is in excellent agreement with the corresponding experimental data[1],[11].

It is clear from the optimized structures shown in Fig.1 and Fig 2 and calculated total energy of these optimized structures that MgO clusters prefer 3-dimensional structures from $(MgO)_4$ onward. A very important observation from the optimized 3-d structures is the chair type structure of MgO clusters from $n \geq 4$. The chair kind structures more clearly visualized in the side views of the structures and more clearly observed in the side views of the fig. 4a, 6a, 6b, 8a, 9, 10. This is very interesting as this indicates the existence of some covalent bonding in MgO cluster where as MgO is considered ionic n bulk state. It is also interesting to note that the optimized planer isomers of MgO clusters have larger angle on Magnesium than Oxygen though the bond length remains same within each plan structure.

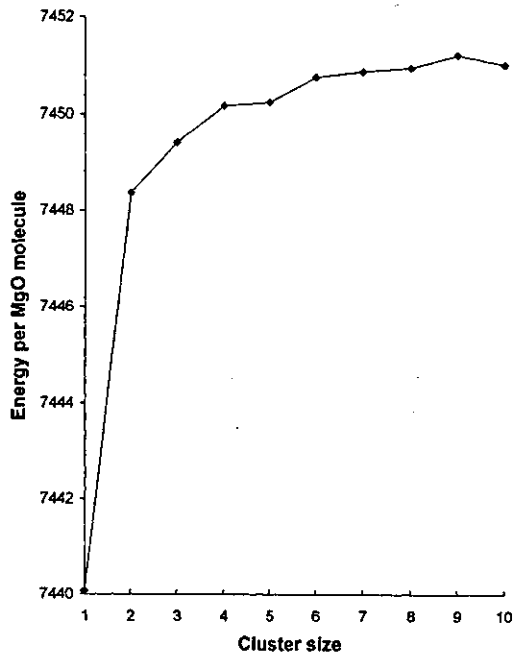

Fig.3 Energy per MgO molecule for the most stable MgO clusters.

The energy per MgO molecule graph with the variation of cluster size, shown in Fig. 3 indicates that Cluster 2, 4, 6 and 9 are more preferable than the other clusters. These results are in full agreement with the mass spectra of MgO clusters[5], which gives the MgO magic clusters at n=2, 4, 6 and 9.

3.2 Parallelized Calculation for MgO Cluster Study

Some *ab initio* simulations for MgO cluster structure optimization have been done on different number of Hitachi SR8000 super computer nodes. Time taken in these simulations has shown the effectiveness of the TOMBO parallelization. A typical comparison of total time taken in structure optimization for $(MgO)_3$ and $(MgO)_9$ clusters when same structure of $(MgO)_3$ and $(MgO)_9$ is optimized with different number of computer nodes in parallel is shown below in Fig. 4

In case of $(MgO)_3$ time saving is not much because time utilized in communicating between different nodes is significant when compared to the actual time saving due to the parallel computation in different nodes. But in case of $(MgO)_9$ there is a significant time saving when number of nodes are increased. The reason for this is that the communication time between different nodes is not comparable to the actual time saving in the computation process due to the use of parallel nodes. As the size of cluster increases, we need more

computational resources and time and we will be able to save more time if using the parallel computing nodes for these larger calculations.

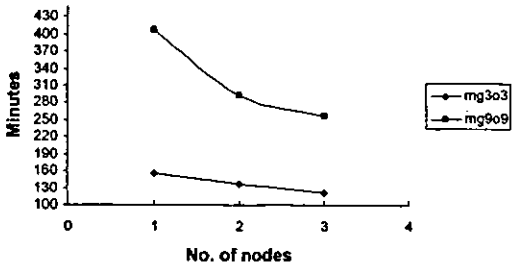

Fig. 4 Time taken for structure optimization of $(MgO)_3$ and $(MgO)_9$ using different number of parallel computer nodes.

4. CONCLUSIONS

In summary, we have reported results of our all-electron mixed-basis calculations using TOMBO. We have reported various isomers and the lowest energy structures of MgO clusters (n=1-10) , which are in excellent agreement with the experimental results available. Another important conclusion of our study from the finally optimized structure is the indication of covalent bonding in MgO clusters whereas MgO is considered ionic in bulk state. We have found magic clusters of MgO at n=2, 4, 6, 9 which are also fully in agreement with the mass spectra. Our calculations also show that the structure optimization through TOMBO is quite fast when used in parallel mode with many parallel computer nodes, which is very important for the further study of large size clusters.

5. ACKNOWLEDGEMENTS

The authors would like to thank the staff of the Center for Computational Materials Science at the Institute for Materials Research, Tohoku University for making the Hitachi SR8000/64 parallel machines available and for their cooperation. We are also grateful for helpful discussions with Dr. Marcel Sluiter and Dr. Umesh V. Waghmare. A. J. is grateful for the support of the Japan Society for the Promotion of Science. V. K. thankfully acknowledges the kind hospitality at the Institute for Materials Research.

6. REFERENCES

[1] J. M. Recio and R. Pandey, *Phys. Rev. A*, 47, 2075-82 (1993).
[2] M.-J. Malliavin and C. Coudray, *J. Chem. Phys.*, 106, 2323-30 (1997).
[3] E. d. l. Puente, A. Aguado, A. Ayuela and J. M. Lopez, *Phys. Rev. B*, 56, 7607-14, (1997).
[4] M. Gutowski, P. Skurski, X. Li and L.-S. Wang, *Phys. Rev. Lett.*, 85, 3145-48, (2000).
[5] P. J. Ziemann and A. W. Castleman, Jr., *J. Chem. Phys.*, 94, 718-28 (1991).
[6] T. Bredow, G. Geudtner and K. Jug, *J. Chem. Phys.*, 105, 6395-400 (1996).
[7] S. G. Louie, K.-M. Ho and M. L. Cohen, *Phys. Rev. B*, 19, 1774-82 (1979).
[8] P. Bendt and A. Zunger, *Phys. Rev. B*, 26, 3114-37 (1982).
[9] Marcel Sluiter, "TOMBO Tohoku University Mixed-Basis Program version 1.2c for Clusters", http://www-lab.imr.edu/~marcel/tombo/tombo.html, (2003).
[10] Marcel H. F. Sluiter, Rodion V. Belosludov, Vladimir R. Belosludov, Amit Jain, Hitoshi Adachi, Yoshiyuki Kawazoe, Kenji Higuchi, and Takayuki Otani, "Ab initio Study of Hydrogen Hydrate Clathrates for Hydrogen Storage within the ITBL Environment," Lecture Notes in Computer Science, Springer-Verlag Heidelberg, Germany, (2003), Vol 2858, pp. 330-341.
[11] K. P. Huber and G. Herzberg, "Molecular Spectra and Molecular Structure,IV. Constants of Diatomic Molecules", Van Nostrand Reinhold, New York, (1979).

(Revised Jan. 7, 2004; Accepted March 31, 2004)

Transactions of the Materials Research Society of Japan 29 [8] 3723-3725 (2004)

Dielectric Function of $(CdSe)_{13}$ Clusters

Yoshifumi Noguchi[1], Kaoru Ohno[1,2], Vijay Kumar[3,4], Yoshiyuki Kawazoe[3], Yurii Barnakov[2], and Atsuo Kasuya[2]

[1]Department of Physics, Graduate School of Engineering, Yokohama National University, 79-5 Tokiwadai, Hodogaya-ku, Yokohama 240-8501, Japan
Fax: 81-45-338-3020, e-mail: d02gd224@ynu.ac.jp, ohno@ynu.ac.jp
[2]Center for Interdisciplinary Research, Tohoku University, Aramaki, Aoba-ku, Sendai 980-8578, Japan
Fax: 81-22-217-5756, e-mail: kasuya@cir.tohoku.ac.jp
[3]Institute for Materials Research, Tohoku University, 2-1-1 Katahira, Aoba-ku, Sendai 980-8577
Fax: 81-22-215-2052, e-mail: kumar@imr.edu, kawazoe@imr.edu
[4]Dr. Kumar Foundation, 45 Bazaar Street, K.K. Nagar (West), Chennai 600 078, India.

We investigate theoretically the atomic and electronic structures of $(CdSe)_{13}$ cluster which is of the smallest magic number size among $(CdSe)_n$ found experimentally recently. Using the first-principles approach based on the local density approximation in the density functional theory, we calculate the dielectric function for two cluster geometries of $(CdSe)_{13}$ and compare the results with the changes in the optical absorption spectra under the illumination.

Key words: optical absorption spectra, dielectric response function, density functional theory, first principles

1. INTRODUCTION

Quite recently, $(CdSe)_n$ clusters have been synthesized and characterized by the optical and time-of-flight (TOF) mass measurements by Barnakov *et al.*[1,2]. The TOF mass spectra of positive ions show that $(CdSe)_{13}$ is an abundant magic number cluster. Kumar *et al.* [3] have determined the most stable geometry of the clusters by means of the standard *ab initio* pseudopotential approach based on the local density approximation (LDA) in density functional theory. The magic $(CdSe)_{13}$ cluster has an endohedral cage structure composed of twelve Se ions at the surface of an icosahedral cage, one Se ion at the center and thirteen Cd ions at slightly inner than the cage surface. The main interest of these clusters lies in their specific behavior in the optical response.

In the present paper, we calculate, for the first time, the dielectric function of $(CdSe)_{13}$ and compare the results with the optical absorption spectra measured by Kasuya *et al.* [1]. In addition to the most stable cage structure, we consider another structure of $(CdSe)_{13}$ which can be obtained by cutting the bulk wurtzite and by optimizing their geometrical structures. Throughout this paper, we use *ab initio* methods within the LDA in density functional theory.

2. EXPERIMENT

$(CdSe)_n$ clusters was created by following sequence :

i . Solution of CdNTA and Na_2SeSO_3 was mingled with decylamine $(CH_3(CH_2)_9NH_2)$ as surfactant.
(Cd^{2+} and Se^{2-} was created in solution)

ii . Toluene was added to the above mixture at temperature of 45℃.
(The clusters grew up in nearby boundary face of toluene and solution.)

iii. The resultant greenish yellow solution of toluene was concentrated and aged for a week.

The optical absorption spectra of $(CdSe)_n$ were measured in toluene after illumination by xenon lamp combined with a monochromater to observe photo illumination effects.

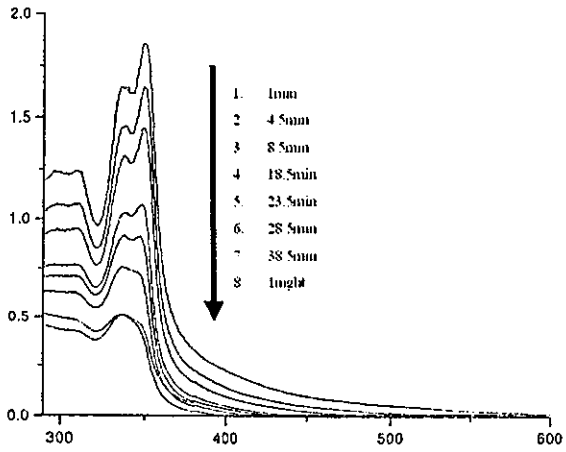

Fig. 1 Optical absorption spectra measured for the $(CdSe)_{13}$ sample in toluene. The abscissa is the light wavelength in units of nm and the ordinate is in arbitrary units. The eight curves (from up to bottom) correspond, respectively, to the observations after 1 min, 4.5 min, 8.5 min, 18.5 min, 23.5 min, 28.5 min, 38.5 min and 1 night light illumination of tungsten lamp after dissolving $(CdSe)_{13}$ in the solvent.

Figure 1 shows the optical absorption spectra of $(CdSe)_{13}$ clusters. The clusters also have the surfactant molecules, decylamine. It exhibits sharp peaks around 340-350nm. The eight curves in this figure represent the change of the observed spectra with the illumination times given in the figure. The uppermost curve is the